Supplementary Materials for

Late Pleistocene Human Skeleton and mtDNA Link Paleoamericans and Modern Native Americans

James C. Chatters,* Douglas J. Kennett, Yemane Asmerom, Brian M. Kemp, Victor Polyak, Alberto Nava Blank, Patricia A. Beddows, Eduard Reinhardt, Joaquin Arroyo-Cabrales, Deborah A. Bolnick, Ripan S. Malhi, Brendan J. Culleton, Pilar Luna Erreguerena, Dominique Rissolo, Shanti Morell-Hart, Thomas W. Stafford Jr.

*Corresponding author. E-mail: paleosci@gmail.com

Published 16 May 2014, *Science* **344**, 750 (2014)
DOI: 10.1126/science.1252619

This PDF file includes:

MATERIALS AND METHODS

The Hoyo Negro Site and its Regional Context

Site description

Hoyo Negro (HN) is a large, submerged, underground chamber of Outland Cave, located 20 km N of Tulum, Quintana Roo, Mexico (Fig. S1). It was discovered in 2007 during an exploration of the Outland Cave by Alejandro Alvarez, Alberto Nava Blank, and Franco Attolini of the Proyecto Espeleológico de Tulum (*26-27*). HN is a bell-shaped chamber (the pit) located below the confluence of three horizontal passages with floors at ~12 mbsl (Fig. 1). The pit is 37 m in diameter at its rim, expanding to 62 m at the boulder-strewn floor, which slopes from 33 mbsl on the north to ~48 m along the south wall. This geometry made it an inescapable natural trap (Fig. S2). HN contains layered fresh and saltwater, with the halocline lying at 15 to 22 mbsl. The freshwater lens is slightly acidic (pH 6.8) and cool (25.2°C), the saltwater is over 95% marine salinity, slightly basic (pH 7.1), and slightly warmer (25.5°C).

The perimeter of the dissolution-fluted floor is variably coated around its perimeter by discrete piles of bat guano and in the center and north side by low cones of calcite-raft sediment. Guano piles formed beneath larger hollows in the HN roof and walls, most as subaqueous accumulations. Walls are marked by distinct color bands that are not attributable to stratigraphic boundaries. The unmodified gray limestone is present below 47 mbsl, above which is an increasingly dark yellowish-brown color to 41 mbsl that we attribute to iron oxides. The dark yellowish-brown band, which we have seen at the water table in nearby subaerial caves, is darkest between 41 and 44 mbsl (Fig. S3). Above 41 mbsl is a narrow band of charcoal, above which the walls are coated in white calcite that is occasionally marked by narrow, light yellowish-brown bands. Charcoal, wood and plant fiber are common on the floor and in hollows and projections along the walls.

Paleontology

The paleontological record of HN consists of plant macrofossils (wood, plant fiber, and seeds from bat guano deposits), and the bones of bats, fish, and large mammals. We have not yet initiated studies of wood and fiber, but our preliminary identification of seeds collected from bat

guano piles indicates they are from tropical fruit-bearing trees, including *Byrsonima sp., Coccoloba sp., Manilkara sp., and Thevetia peruviana,* which are still common in jungles of the northern Yucatan Peninsula. Fossils of 11 large mammal species (Table S2) are found in the tunnels (*Tapirus,* cf *Cuvieronius, Smilodon*) and in the southern one-third of the HN floor, below 40 mbsl (Fig. S4). Except in the southeastern-most portion of the floor, where no boulders or wall projections exist, the shallowest elements from each large animal lie between 39.8 and 43.0 mbsl. With few exceptions (one *Nothrotheriops*, two *Puma*) elements of each individual are scattered in semi-articulated, often widely separated groups, a pattern consistent with decomposition while the carcasses floated in water (*28*). Long bones of at least five individuals (*Puma, Smilodon, Tayassu,* megalonychid ground sloth) exhibit perimortem fractures resulting from impact with a hard surface during their fall into HN, either onto a dry floor or into shallow water. Even the surface of the water could have caused some of the fractures after a 30 meter fall.

We have, to date, studied Hoyo Negro's human and animal fossils remotely, in much the same way NASA scientists studied the moon. The fossils lie at more than 40 m below the water surface in a lightless, drowned cave. Work in this dangerous environment requires technical skills and experience our anthropological and paleontological members lack. We cannot, therefore make direct observations, but guide the collection of images and data by those members who have the necessary experience. We have left most fossils in place, for multiple reasons. Extraction, especially of large or delicate specimens, is mechanically challenging in a submerged cavern environment. Once specimens are removed, they must be transported wet over 7 km of rugged terrain, then undergo prolonged desalinization before they can be stabilized. These activities are currently cost and time prohibitive. In addition, ethics of the cave diving community require the divers to leave conditions exactly as they are found. While this refers primarily to geologic formations, it has become extended to fossil remains. Violating this ethic would compromise the collaboration between divers and scientists on this project. Finally, facing these conditions, we are attempting to establish a new standard for minimally invasive scientific research in a delicate, dangerous environment, replacing collection with videography, high-resolution scaled photography and 3-dimensional modeling.

Bones and bone concentrations were located, given specimen numbers, and photographed by the dive team. We made field identifications from these photographs with reference to

comparative specimens and published holotypes, and confirmed them in consultation with taxonomic experts. With the exception of one molariform tooth from a gomphothere (see Sampling), one *Tremarctos* mandible, and a sternal rib from a ground sloth, all skeletal material remains *in situ*.

Geological and paleoecological context

The Yucatan Peninsula is a low-topography carbonate platform with off-lapping sequences. The central Paleocene-Eocene limestone grades outwards to early Pleistocene coastal margins (*29*). The peninsula is highly karstified, such that surface streams and rivers are absent from the whole northern lowland, leaving groundwater as the only natural source of potable water (*30-31*). The regional hydraulic conductivity (permeability) is high at 10^{-1} m/day (*30*), consistent with other highly karstified coastal aquifers (*32*). The hydraulic gradient is consequently exceptionally low at 10^{-5} (unitless), which equates to a rise of 1-10 cm over a km distance (*30*). Sea level is the most significant boundary control on the whole aquifer system, with the water table nearly directly tracking changes in sea level with only a small vertical offset of 1-2 m within ~100 km of the Caribbean coast (*30*). Extensive perched water tables are not sustainable in this highly karstified aquifer. While some indurated sub-aerial surfaces, locally called caliche, create semi-confining conditions on the north coast (*33*), there are no reports to date of similar semi-confining conditions along the Caribbean coast. This may relate to local fracturing, dissolution, and collapse, often forming sizeable underground pits (such as Hoyo Negro), as well as the influence of the extensive and deep Holbox bank-marginal fracture system that runs parallel to the Caribbean coast (*30-31*).

The caves of the Yucatan Peninsula formed subaqueously at levels tied to past sea level stands (*31*) and were drained during the late Pleistocene when sea levels lowered by as much as 110 m in response to changes in the mass of glacial ice. Cave diving exploration focused on the eastern margin has revealed dense, stacked, horizontal conduit networks, of which the shallowest cave level lies ~10-15 m below the modern water table (*31, 34*). One of these flooded systems is Sac Actun, which includes Outland Cave. The second longest submerged cave system in the world, Sac Actun consists primarily of submerged speleothem-draped horizontal passages within ~23 m of the modern ground surface. The system is marked by numerous sinkholes (cenotes) that connect submerged tunnels with the surface. Each of the horizontal passages is reachable

from one or more cenotes from which large animals could have entered the caves. In the case of HN, Cenotes Oasis and La Concha are the nearest sinkholes large enough to have permitted entry by large mammals, and both lie more than 600 m from the underground HN pit (Fig. S1). The passage from Oasis is high (>3 m) and wide enough along its entire length for the movement of animals the size of a gomphothere. Other, nearer sinkholes might have existed in the past, but none has yet been recognized. The nearest sinkhole is Ich Balam, a 1.2 by 5 m crevice, which is located 60 m downstream of HN. Our initial coring efforts in the Ich Balam debris cone indicate it has been open for 8000 years and likely longer.

At lower sea levels, the shallow tunnels were air-filled above the water table and accessible to animals. With lower water levels and reduced evaporation from a cooler sea surface, the now-humid, tropical climate was at times much cooler and drier (*35*-*37*). A deep sediment sequence from Lake Petén Itza, 500 km to the southwest in the climatically similar Petén region of Guatemala provides a record of full-glacial to early Holocene environments. Pollen and sediment composition indicate mesic climate and a temperate pine-oak forest from 23 to 18 ka, aridity and a thorn scrub/savanna from 18 to 10.3 ka, with a slightly wetter interval between 14.7 and 12.8 ka, and more mesic tropical forest after 10.3 ka (*38*-*39*). The monsoon over Mesoamerica was weakened at around 17 ka and during the Younger Dryas (*35*). Although people of a distinctly different cultural tradition were already well established in South America (*40*), the earliest cultural tradition that has been documented in southern Mexico and Central America is Clovis, which arrived shortly after 13 ka (*41*). Sites and isolated projectile points of the Clovis tradition have been documented in Panama, Costa, Rica, Belize, and Guatemala (*41*). However, no Pleistocene-aged archaeological site has yet been found in the Yucatan Peninsula due in large part to a focus on Maya prehistory.

The karst systems of Yucatan are known to contain remains of Pleistocene megafauna, and human remains dating to the Mayan culture and Archaic period (*42*-*43*). Eight other sets of apparently pre-Maya human remains have been found in the caves of the Yucatan Peninsula Quintana Roo (*43*), but although claims of great antiquity have been made for the Naharon woman (13.4-13.8 ka; *44*) the expert who produced the apparent age measurement does not consider the result to be valid (*45*).

Sampling Methods

Specimens for ^{14}C, U-Th, and aDNA analyses were obtained in the following manner, by material type.

Bone and tooth sampling

Three human skeletal elements and one gomphothere tooth were removed from HN in 2011 and 2012. After inspection of photographs of *in situ* materials, individual specimens were designated for collection based on their accessibility and suitability for radiocarbon and/or aDNA analysis. A human upper central incisor (Fig. S7, F) was loose, at risk of falling into an inaccessible crevice, and was collected; the human's left third molar (Fig. S8, A-C) was selected for analysis because its crown appeared intact and consequently had a high potential for preserving aDNA. The simple root structure facilitated removal without damage to alveolar bone. The human's left 12^{th} rib lay un-obscured and was small enough to survive being lifted even if. A *Cuvieronius* molariform (Fig. S9, D), which had the potential for intact collagen in its dentine, lay unobstructed near the human mandible. Designated elements were pre-numbered on laminated photographs for collection. Divers identified these elements and, wearing peroxide-sterilized, un-powdered, nitrile gloves placed them and surrounding salt water into peroxide-sterilized re-sealable bags and capped test tubes for extraction. Once removed from the water, specimen containers were kept unopened; except during transport, the samples remained refrigerated at 4°C. The human molar was not exposed to air until it reached the sterile environment of the Washington State University ancient DNA laboratory.

Bat guano sampling

Guano is found around the margins of HN in conical accumulations. Lying below hollows produced by prolonged use by roosting bats, containing seeds of plants foraged by fruit bats, and closely resembling guano deposits seen today beneath active bat roosts, this guano is positively identifiable as bat droppings. Divers collected seeds and amorphous organic material from the apices of four guano piles for ^{14}C dating. The goal was to determine when guano deposition ceased. Guano was also encountered during coring of a calcite raft cone in the pit center by McMaster University. Located below the raft sediment, this guano was found to contain freshwater-dwelling ostracods and thecamoebians. Based on our observation of cores in

Ich Balam, the presence of these organisms represents deposition in shallow meteoric water as the sea level continued to rise, with the overlying raft material representing the deepening phase. Because of this association, we selected two seeds from the uppermost organic stratum in the lowest part of this core for ^{14}C dating to determine a minimum age for sea level flooding of the deposit's elevation, 42 mbsl.

Sampling of calcite florets

Bush-like overgrowths of $CaCO_3$, referred to hereafter as florets, are densely scattered over the boulders on which HN5/48 and gomphothere 1 (HN-6/7) lie. These were determined to be calcite using Raman spectroscopy. Divers have observed them only in this area, around and between a scatter of flat-topped stalagmites that stand below a curtain of stalactites on the chamber's ceiling (Fig. S2). Close inspection of project photographs supports that observation. Two floret forms are present: 1) rounded, bushy speleothems stained dark yellowish-brown (Figs. 2, S10) that tend to be relatively rare, and 2) smaller, white, trianguloid branches that form a near-continuous carpet above ~41.5 m. Darker florets seen on photographs were in upright position on human and gomphothere bones when selected, numbered, and marked on waterproofed prints. Their upright position was taken as evidence of formation *in situ*; a similar assumption could not be made for the smaller, light-colored florets. Designated specimens were on the surface of the human mandible, scapula, rib, femur, and os coxae, and on the gomphothere femur and innominate. Two large florets that had formed on limestone surfaces were also collected near the human skull. The purpose was to determine if they differed in age from the florets found in skeletal contexts. Divers matched specimens with numbered images and collected them in pre-labeled, screw-cap, plastic jars. The location of each specimen was photographed post-collection to observe the condition of the bone beneath it. We observed that bone surfaces that had lain in contact with another object since their deposition were uniformly white, whereas all others were dark reddish brown. Although a thin calcite film could be seen beneath the collected florets, indicating their former residence, all bone surfaces were darkly stained, indicating they had lain exposed on the cave floor for some time before the florets began to form.

Radiocarbon Analysis

AMS ^{14}C measurement of enamel bioapatite (Stafford Research Laboratories Inc.)

Enamel bioapatite from the right upper 3rd molar of HN5/48 (HN111205-3) and the associated gomphothere (*Cuvieronius* sp.; HN120512-24)(Fig. S9) was submitted to Stafford Research Laboratories Inc. for AMS ^{14}C measurement. Samples were cleaned of dentine and adhering detritus using a razor blade and dental pick. In cross section, the human molar exhibited a 10-50 μm thick, iron-stained outer surface and a clean, translucent interior; the enamel from the gomphothere had a thicker outer patina, thin iron-stained laminae penetrating into the enamel at an angle approximately perpendicular to the outer surface, and secondary staining along the contact with the dentin. The initial mass of the samples was 252.1 mg for the human and 310.0 mg for the gomphothere. Both samples were broken into 1-to-2 mm fragments and subsequently etched in an excess of 0.6 *N* HCl at room temperature to remove secondary carbonates. The reaction was closely watched under binocular microscope until ~10% of the enamel's mass was removed. Iron-rich surface residues were observed to separate from the enamel as flexible, thin sheets. Etched enamel was rinsed in deionized water and lyophilized. A sample of Harding pegmatite calcite was processed by these same methods as a ^{14}C background. The dried samples were placed in acid-washed glass vials and submitted to the Keck Carbon Cycle AMS Facility (KCCAMS) at the University of California, Irvine for digestion, reduction to graphite, and AMS ^{14}C measurement using standard methods (*46*). Upon submission, the HN111205-3 split weighed 124 mg and HN120512-24, 238 mg. Both were first etched to 75% their remaining mass in HCl (reducing original mass by a total of 32%) and hydrolyzed in 65% phosphoric acid, producing C yields of 0.67 mg and 0.75 mg, respectively.

AMS ^{14}C age confirmation of enamel bioapatite (Pennsylvania State University)

Enamel bioapatite splits from HN-111205-4 and 120512-24 were processed at Pennsylvania State University (PSU, Human Paleoecology and Isotope Geochemistry Laboratory) for AMS ^{14}C dating by acid hydrolysis. Samples were cleaned with dental tools to remove adhering residues, and dentine was removed from the gomphothere tooth with a combination of dental pick and drill. Both samples were acid-etched to remove secondary carbonate prior to hydrolysis. The human molar (114.97 mg) was etched in 3 ml 0.1 *N* HCl at 80°C until completion, at which point ~15% of the mass had been removed. The gomphothere

enamel (233.35 mg) was etched in 4 ml 0.5 *N* HCl, resulting in a ~60% mass loss. A calcite background and IAEA-C2 travertine secondary were acid-etched (50%) in 2.2 ml 0.1 *N* HCl; an additional secondary standard, the FIRI-C turbidite, was not etched. After rinsing in Nanopure H_2O and drying at 50°C, samples and standards were placed in BD Vacutainer septum-stopper vials, and digested with 85% orthophosphoric acid following protocols of the Keck Carbon Cycle AMS laboratory (*46*). Estimated final C yield was 0.56 mg for the human, and 0.57 mg for the gomphothere. The CO_2 generated at PSU was sent to KCCAMS for reduction to graphite, using that facility's standard procedures (*47-48*).

Graphites from enamel pretreated by Stafford Research Laboratories Inc. and PSU were measured in the KCCAMS facility. All ^{14}C ages were $\delta^{13}C$-corrected for mass dependent fractionation with measured $^{13}C/^{12}C$ values (*49*). Conventional ages were calibrated with OxCal v 4.2 (*50*) updated to the IntCal13 Northern Hemisphere atmospheric curve (*25*).

AMS ^{14}C measurement of bone apatite: DirectAMS

A split of the rib from HN5/48 (HN-111204-2) was processed at the DirectAMS radiocarbon preparation laboratory in Bothell, Washington. Because bone is more subject to contamination from dissolved inorganic carbon (DIC) than tooth enamel, it provides a measure of the direction such contamination could take the age of the enamel. Under magnification, the rib tissue exhibited a light, grayish-brown color with extensive $CaCO_3$ infilling of vascular canals. Contamination from DIC was clearly pervasive. Its surface was coated in a similar iron-based stain to that seen in the enamel, but the penetration of the stain was more than 10x deeper. The initial mass of the sample was 357 mg. The outer iron stain was scraped away with dental tools and the sample broken into 1-to-2 mm fragments. Fragments were soaked for 24 hr in consumer-grade peroxide, washed repeatedly in deionized water, leached for another 24 hr in 1.2 ml of 1 *N* acetic acid, rinsed to neutrality, and oven dried at 90°C. At this point the sample was again weighed (308 mg), then etched to completion in 9.3 ml 0.1 *N* HCl at room temperature to remove more of the secondary carbonates. Etched bioapatite was rinsed in deionized water, lyophilized, and weighed. Etching removed 22% of post-acetic-leach mass, leaving 239 mg of material. The sample was then hydrolyzed under vacuum in 1.0 *N* phosphoric acid and graphitized following the laboratory's standard procedures (*51*). The sample yielded approximately 1.1 mg of final C.

Bioapatite ^{14}C measurement results and discussion

Human enamel produced ^{14}C ages of 10,970±30 RC BP (12,970-12,655 cal BP at 2σ,SR-8205/UCIAMS-119438) and 10,985±30 RC BP (12,985-12,670 cal BP at 2σ, PSU-5493/UCIAMS-123541)(Table S3). These were averaged using the method of Ward and Wilson (*52*) to produce a mean age 10,976±20 RC BP (12,910-12,720 cal BP at 2σ). This statistically indistinguishable result, despite differences in the pretreatment protocols (etching after fragmentation versus etching entire and 55% vs. 15% removal by acid etching) provides a level of confidence in this age determination. The gomphothere samples produced measurements of 36,250±370 RC BP (SR-8206/UCIAMS-119439) and 33,590±370 RC BP (PSU-5493/UCIAMS-123542). The sample of the human rib bioapatite produced a radiocarbon age of 16,164±78 RC BP (DAMS-4981).

Bioapatite is a less than ideal material for radiocarbon dating (*53*), particularly in more mesic contexts (*54*) because bioapatite is susceptible to both physical contamination with $CaCO_3$ and solid-phase replacement of CO_3-^{2} in the hydroxyl-carbonate-apatite (dahlite) crystal lattice. Although such contamination usually results in younger age measurements (*54, 55*), either type of carbonate contamination could cause the sample to date older than its actual geologic age if the dissolved inorganic carbon (DIC) in the surrounding water contains a high proportion of fossil carbonate. Bone apatite, which occurs in small crystals residing in a highly porous matrix of vascular canals and channels left by decomposed collagen, is much more subject to contamination than the larger crystals and nonporous matrix of tooth enamel (*54*). Hence, the direction a radiocarbon date on bone bioapatite takes from the enamel age—whether younger or older—informs about the direction contamination, if it had occurred, would take the apparent age of the enamel. This determines whether the enamel age should be considered a minimum (younger bone) or maximum (older bone) possible age. In this case, the statistically identical ages obtained by different processes gives us some confidence in the enamel age as the true age of the human skeleton because the random process of contamination should lead to divergent results, as seen in the gomphothere tooth, not to convergence. The probability that the ages match because they represent the true age is far greater than that they match as a result of precisely equal levels of contamination. However, because the DIC in water that surrounded the teeth clearly contained a significant level of fossil carbon, present evidence requires that we consider this a maximum age for the skeleton.

Discussion of a potential marine reservoir effect

We estimate the maximum potential marine reservoir effect for the region to be in the range of 400±100 ^{14}C yr using reported estimates in Reimer et al. (*25*:1115, Table 1). However, the potential that a marine reservoir effect impacts the age estimate for HN5/48 is low, for three reasons. First, dental attrition (see Human Osteology) in the HN human is unusually light for a hunter-gatherer consuming food containing sand-contaminated fish or shell fish; that is, a marine-based diet. In our experience with skeletal material from the Pacific Northwest of the United States, where marine and riverine diets prevail, dental wear by age 16 is significantly greater than for the HN human. Second, dental caries and enamel pitting seen in the upper first incisor are indicative of a diet having abundant fruit content, that is, a terrestrial diet. Finally, paleoecological studies of Central America suggest that Paleoindians were focused on terrestrial game and forest plant resources. A marked increase in charcoal at ~13 ka has been interpreted as Paleoindians burning the forest to benefit human food species (*56*).

XAD-purification of dentine protein

We attempted at both laboratories to extract collagen or amino acids from human and gomphothere samples. At PSU, these attempts for the human addressed, first, the human rib (HN-111205-2; 2 attempts) and later the root dentine of the upper central incisor (HN-111205-1). Visual inspection and a CT scan (rib only) indicated that these samples were heavily mineralized; therefore, we used modified protocols established by Stafford et al. (*57*). Bone and tooth samples were physically cleaned to remove staining and the outer surfaces. Cleaned samples (~200-400 mg) were placed in 20 ml scintillation vials with ~10 ml 0.2 *N* HCl and the samples were decalcified at 4°C over 3 days. Decalcified samples yielded a 0% pseudomorph (cf. *57*, Table 1). Because of the poor preservation, no KOH washing was attempted. The residue was subjected to gelatinization and hydrolysis, producing a residue that had the appearance of salts rather than organic material. Carbon and nitrogen content measured on an elemental analyzer were close to or indistinguishable from zero for all samples. Dentine from the gomphothere produced the same results.

At Stafford Research we attempted to extract collagen or amino acid residues from dentine of the human and gomphothere molars (HN-111205-3 and 120512-24). Visual inspection showed chalky, mineralized gomphothere dentine; human dentine had a chalky interior and more

dense dentine in contact with the enamel (Fig. S9, D). Samples (~175-300 mg), which came from tooth interiors, were demineralized in 0.6 *N* HCl at 4°C for 24 hr. No collagen pseudomorph was observed. Residues were hydrolyzed in 6 *N* HCl at 110°C for 24 hr, producing only organic salts which, when tested for protein using a quantitative amino acid analysis, contained only 1.7-2.1 ng amino acids/mg dentine. Modern dentine contains ~2500 ng/mg.

Uranium-Thorium Analysis

Brief sample description

The samples collected and analyzed were speleothems growing on and near human and gomphothere bones. These speleothems are similar to calcium carbonate 'bushes' or 'frostwork' that are commonly aragonite rather than calcite (*59*) and are termed 'florets' in this study. The florets appear to grow like a bush or tree from a single trunk (Fig. S11). The crystals are not acicular like those of frostwork, which may be because the florets are calcite rather than aragonite. The calcite crystals branch from the trunk. They are 40-50 mm at most in diameter. The larger samples that were collected consisted of dense white calcium carbonate. Most are stained with a yellowish-brown film of presumably Fe-bearing organic material. The smaller samples were more fragile and porous and less suitable for U-Th analyses.

First U-Th results from 'clean-looking' untreated sub-samples

The first analyses were of four pieces of sample HN-7 that lacked the yellowish-brown staining. Because they were minimally stained, they were measured without pre-treatment. U-Th results indicated a ^{230}Th-^{234}U-^{238}U isochron age (*60*) of 14.4 ± 1.6 ka (Table S5), with the assumption that all four samples were the same age. The absolute large error on these results indicated that detrital ^{232}Th was interfering with measurement of an accurate age. Experimenting with etching of samples HN-15-1, HN-15-2, and HN-17-1b indicated that the dark yellowish brown stain on the florets and/or a thin corroded layer was contributing most of the detrital ^{232}Th, and introducing significant amounts of 'extra' ^{230}Th that did not result from the radioactive decay of U in the calcite.

Pre-analysis processing to remove ferric staining and corroded layer

Ammonium hydroxide, acetic acid, and nitric acid were experimentally used to remove the altered surfaces; nitric acid efficiently and quickly removed the stain and any corroded exterior that would interfere with the accuracy of our measurements. A treatment of 0.5 to 1.5 minutes of 0.5 *N* HNO_3 was necessary to remove the stain and corrosion layer. The samples were monitored visually and treatment was stopped when only clear, crystalline material remained. After treatment, samples were washed three times with 18 M-ohm water. Approximately 10-35% of the raw sample was dissolved during this treatment, depending on the time needed to dissolve the stain. This treatment removed the yellowish-brown film, any corroded layer, and some of the calcite. Leachates were collected and analyzed as well. A test was conducted on calcite having a similar age and U concentration as the florets, and showed that processing with 0.5 *N* HNO_3 for 1 minute had no significant effect on the age measurements (see Fig. S12). In addition, Fig. S11 shows the dark yellowish brown stain on the samples and the pure white samples after treatment.

Dark yellowish brown stain and corrosion layer contain higher concentrations of ^{232}Th and 'unsupported' ^{230}Th

Etched and cleaned samples consistently produced ages between 12 and 9.6 ka, all with small absolute errors (Table S4). These treated and cleaned samples had much less detrital ^{232}Th. The leachates of these produced much higher ages and greater amounts of ^{232}Th (Table S5), showing that the yellowish-brown stain and/or corrosion layer has a much higher initial ^{230}Th/^{232}Th ratio than does the calcite. U-Th results from treated sub-samples having >3000 ppt of ^{232}Th were separated and considered suspect for causing anomalously high ages. However, all results from the experimental work to set up a pre-analysis treatment method, all results having ^{232}Th higher than 3000 ppt and those untreated samples having anomalously high ages are included in Table S5.

U-Th and Sr-isotope chemistry

The U-Th separation chemistry is described in Asmerom et al. (*61*). Florets weighed between 10 and 120 mg before analysis and were dissolved in 15 *N* HNO_3, then spiked with a mixture of ^{229}Th, ^{233}U, and ^{236}U, and fluxed at moderate heat for one hour. U, Th, and Sr were

separated using Eichrom 1x8, 200-400 mesh chloride-form anion exchange resin. An additional column step using Eichrom Sr-spec resin was used to cleanly separate Sr. All samples were analyzed on a Thermo Neptune multi-collector inductively coupled plasma mass spectrometer (MC-ICP-MS). Standards NBL-112, NBS-987, and an in-house ^{230}Th-^{229}Th solution were analyzed several times during the run sessions.

More accurate radioactive half-lives for ^{230}Th and ^{234}U, and improved MC-ICP-MS analytical methods were used in this study (*62*). U-series age corrections were based on the analyses of three sub-samples of a floret that was small and had only branched once (HN130219-14, Fig. S11). Because the small floret had only branched once, it is likely that all three pieces yielded ages that are sufficiently close to each other that an isochron could be constructed. The U-Th results of these three sub-samples produced a ^{230}Th-^{234}U-^{238}U isochron age of 11.3 ± 0.6 ka, and yielded an initial ^{230}Th/^{232}Th atomic ratio of 32 ± 16 ppm (activity ratio = 5.9). This atomic ratio and its 2σ absolute error were used to calculate the corrected ages for all other results.

Radiogenic isotope evidence pertaining to the origin of the florets

The δ^{234}U and ^{87}Sr/^{86}Sr values for the etched florets, their leachates, HN5/48's upper right central incisor, a soda straw stalactite, and the brackish water are shown in Fig. S13 and Table S4. These data are an indication that the florets did not form from seawater and it is not likely that they formed from brackish water. The data are an indication that the leachates formed in brackish water; the dark yellow brown stain was probably deposited while submerged in brackish water. The δ^{234}U and ^{87}Sr/^{86}Sr values of the soda straw, human tooth, and florets also suggest that the water related to the origin of these is from early to middle Miocene limestone (*63*), or a soil contribution that produces a water with early-middle Miocene limestone values. The age of the florets shows that they grew when sea level was below 42 mbsl. The morphology of the florets and their isotopic compositions support their formation in a subaerial environment; however, the florets could have formed in perched pools fed by drip water.

Human Osteology

General description of the skeleton's context

HN5/48, the human skeleton found in Hoyo Negro, lies scattered over an area 5 m long by ~1.5 m wide near the east-center of the chamber floor (Fig. S4 and S6). It lies along the southern edge of three large boulders, in four groups. From west to east, these are the pelvic girdle (group 48); right arm and left forearm, with a few thoracic vertebrae and ribs; skull, left scapula, upper right shoulder girdle, and a few cervical vertebrae and ribs; and a final cluster of four ribs (Fig. S6). All of these groups lie at between 41.5 and 42 mbsl. Three additional ribs lie scattered among bones of *Cuvieronius* 1 (HN-6/7) at the bottom of a deep cleft ~47 mbsl. We argue that the scatter of bones in anatomical groups resulted from decomposition of a floating corpse (*28*) in floodwater that temporarily filled the chamber. Occurrence of the majority of elements at the same elevation across the skeleton's entire horizontal extent marks the temporary water surface at the time of decomposition.

Methods of observation

Only four elements of HN5/48 have been removed from the water. Therefore, most observations are based on scaled, high resolution, underwater digital photographs. Photographs of the skull were taken on two occasions using a tripod-fixed Canon 7D SLR with a Canon 50 mm 1.8 lens and YS250 Sea strobes, with the skull resting on a similarly fixed turntable. Photos were taken at 20° intervals with the skull in both inverted and upright positions. Additional images were made of the cranial base and in superior view, with the camera off-tripod structure-from-motion software to generate a scaled, 3-dimensional, digital model of the skull that could be used for qualitative observation and precise craniometry (Fig. S8). To the extent possible in the submerged, topographically complex cave environment, measurement of longbones was accomplished by placing scales either directly on elements or parallel to them in the same plane to maximize accuracy. We made measurements of photos using a Brown and Sharpe TESA® analog sliding caliper. Because measurements made by this latter means were not made directly, such values are approximate and represented by the ~ symbol. Craniometrics are provided only as indices, following Bass (*64*).

Skeletal inventory

To date, we have identified 46 skeletal elements of HN5/48 through inspection of photographs. These are the skull with 14 teeth and the mandible with 14 teeth (missing are left I^1 and I^2 and right I_1 and I_2); left scapula, humerus, radius and ulna; right scapula, clavicle, humerus, radius, ulna and one metacarpal; both os coxae; sacrum; both femora; one tibia; one fibula; six thoracic vertebrae, two cervical vertebrae, and 19 ribs. All bones are in excellent physical condition and are stained a dark yellow-brown. All but two elements were complete and unbroken at the time of discovery. The two os coxae exhibit breaks stained the same dark rust color as other bone surfaces, indicating breakage early in the skeleton's residence in the cave. The os coxae are missing the pubic bones, the absence of which is marked by fractures with sharp edges and acute angles. The shape of the fractures indicates breakage when bone still contained its protein matrix; fracture after protein dissolution would result in crushing of the bone or breaks at right angles to the outer bone surface. Had a falling stalactite caused the breaks, for example, the object and the broken pubic portions of the two os coxae should remain on the level surface where the pelvis lies. No stalactite fragment exists. Despite repeated close examination of high resolution video and multiple photographs, neither of the two pubic bones can be found near the rest of the os coxae, indicating the broken pubic bones fell from the decaying, floating corpse before the rest of the pelvic girdle came to rest. In order to have the dark stain we see today, the broken surfaces of the nasal bones must have been exposed since the skull came to rest. Based on these observations, we conclude the ancient fractures to the os coxae occurred perimortem. Parts of the nasal bones, the zygomatic process of the left temporal, the left humerus and clavicle, and the right scapula are also broken from post-discovery disturbance by unauthorized visitors to the site.

Sex, age, and stature

The skeleton is female. Sex characteristics were scored following forensic standards (*65*). The greater sciatic notch is broad (score 1) and preauricular sulcus well-developed (score 2). Determination of sex in adolescents (see below) can be problematic because evidence of a male pattern in a pelvis could represent a female who had not yet undergone the expansion of the pelvic outlet and retains the preadolescent condition. Identifying an adolescent skeleton as male on the basis of pelvic characteristics is, therefore, equivocal. However, an adolescent pelvis

exhibiting typically female features, can confidently be diagnosed as female (*65*). Skull features are consistent with a female assessment, including the absence of a nuchal crest (score 1), minimally developed mastoid processes (score 1), a sharp supra-orbital margin (score 1), lack of a supraorbital ridge (score 1), a weakly developed mental eminence (score 1) and obtuse gonial angle. Musculoskeletal markings are in all cases weakly developed. In addition, the skeleton appears markedly gracile.

Age of the Hoyo Negro human is based on patterns of dental eruption and epiphyseal union in longbones. All teeth have erupted. Upper third molars are fully erupted but only the right is in occlusal position; the apex of the collected left M_3 was ¾ complete. M_3 crowns are fully formed but the teeth have not erupted, apparently due to impaction. Eruption of the M3 occurs between 15 and 21 years (*66*), the root is ¾ formed between 13.5 and 20.5 years (*67*). The spheno-occipital synchondrosis is partially fused, which places age between 12 and 16 years (*68*). Epiphyses of the distal radius, distal ulna, and iliac crest are fully formed but unfused. Epiphyses of the humeral heads are fused, placing age at $\geq$15 years. Those of the greater femoral trochanter, lesser trochanter, and head of the femur, proximal radius, and medial humeral epicondyle are complete, making this person older than 14 (*68*). One distal femur has a fused epiphysis, the other appears to have been unfused or loosened in the fall that broke the pubic bones; the distal femur is in the process of fusing in females between 14 and 19 years. Fusion of the greater trochanter occurs after 17 years in males and up to two years earlier in females, giving HN5/48 a minimum age of 15 (65, 68, 69). HN5/48 thus can be placed at around 15-16 years of age.

HN5/48 was small. Applying Genoves' (*70*) equation for Mesoamerican females to the estimated full length of the left femur measured by photographing a scale placed parallel with the bone at the same elevation (~38.2 cm), she stood ~148.6±3.8 cm tall. Slender diameters of longbones, which could not be accurately measured from photographs, indicate a very gracile individual.

Pathology and trauma

Skeletal defects observed to date are dental caries and a healed fracture of the radius. Large careous lesions occur on the labial, lingual, and distal interproximal surfaces of the right I^1. The interproximal lesion continues into the adjacent I^2. Small lesions appear to be present on

the left I_2 and M_1 and right M^2, but cannot be confirmed from existing images. Dissolution craters are evident at the cemento-enamel junction and occlusal to the large lingual careous lesion in the I^1, indicating an acidic oral environment consistent with a high fruit diet. The distal shaft of the left radius contains evidence of a long-healed greenstick fracture in the formation of an abnormal angle and the absence of bone callus (Fig. S7, G).

Cranial morphology and dental traits

The maturation of the size and shape of the human skull are complete by 15.7 years of age (*71*), making the 15-16 year-old HN5/48 suitable for comparison with other American crania. HN5/48 has a high (mean height index 90.7), mesocranic neurocranium (cranial index 76.9) with a pentagonal cross-section. The forehead is high and prominent, the occipital angled and posteriorly projecting. The upper face is short and broad (upper facial index 47.4). It is small in comparison to the neurocranium, with bizygomatic breadth smaller than the maximum cranial breadth. Malars are not everted. Alveolar prognathism is moderate and the dental arcade long (maxilloalveolar index 1.08) and parabolic. Orbits are low (orbital index 81.3) and the inter-orbital space broad (23 mm). The nasal aperture is wide (nasal index 53.4). We have seen similar characteristics in the other largely complete crania of Paleoamerican females, including the remarkably similar Wilson Leonard from central Texas (*72*).

All tooth forms are represented. Remodeling of alveolar bone indicates the missing incisors were lost a short time antemortem. Dental attrition is light, corresponding to between Hillson's (*73*) Stages 2 and 3. Dentine is exposed only in upper central incisors and on lower central incisors, one canine, the buccal cusp of the P_1 and the mesio-buccal cusp of the left M_1. Dental traits, scored according to the University of Arizona templates (*74*) include moderate I^1 shoveling (score 4) but no double shoveling (Fig. S7, F); a well-developed distal accessory ridge in the canines (score 4), absence of UtoAztecan premolar; a five cusps plus a prominent Carabelli cuspid (score 5) on the M^1, a 5-cusped M^2, six-cusped M_1, no deflecting wrinkle on the M_1, Y-grooved six cusped M_2, and M3s approximately equal in size to M2s. Winging of I^1s cannot be scored due to contact with the severely maloccluded I^2. Root numbers for P^1 and M_1, and numbers of cusps on P_1 could not be scored due to a lack of visibility in photographs and wear of the enamel. In general, the dentition exhibits a combination of traits included in both the

Sundadont and Sinodont dental complexes (*10*), plus others (Carabelli cuspid) that are in neither, an amalgam of characteristics previously observed in other Paleoamerican dentitions (*75*).

aDNA Analysis

DNA extraction, PCR amplification, and sequencing (Washington State University)

All pre-PCR work was conducted in the ancient DNA facility at Washington State University (WSU), located in a building separate from where PCR is conducted. After separating the crown from the root, 42 mg of the root was removed for DNA extraction. This material was submerged in 6% sodium hypochlorite (full strength Clorox bleach) for 4 min after which it was rinsed twice with DNA-free ddH_2O and moved to a 1.5 mL tube to which 500 µL of EDTA (pH 8.0) was added. This was accompanied by an extraction-negative control of 500 µL of EDTA, to which no sample was added. The tubes were incubated with gentle rocking at room temperature for 48 hours. Sixty units of proteinase K (Biobasic) were added to the tubes and incubated at ~65°C for 3 hours. The volumes were transferred to 5 mL Falcon tubes, to which 750 µL of 2% celite in 6 M guanidine HCl and 250 µL of 6 M guanidine HCl were added. The tubes were vortexed numerous times over a 2-minute period. These mixtures were pulled across Promega Wizard® Minicolumns using Luer-Lok syringes and a vacuum manifold. The silica pellets were rinsed by pulling 3 mL of 80% isopropanol across the columns. Residual isopropanol was removed from the columns by centrifugation in 1.5 mL tubes at 10,000 rcf for 2 minutes. The columns were moved to new 1.5 mL tubes and 50 µL of 65°C DNA-free ddH_2O was added to the column and left for 3 minutes prior to centrifugation at 10,000 rcf for 30 s. This step was repeated, resulting in 100 µL of extracted DNA.

The extracted DNA was first tested for PCR inhibitors (*76-78*). As this sample did not require further purification, characteristic markers of Native American mitochondrial DNA haplogroups A-D were screened [*Hae*III at nucleotide position (np) 663 (+), the 9-bp deletion, *Alu*I at np 13262 (+), and *Alu*I at np 5176 (-)] according to Kemp et al. (*5*). A portion of the first hypervariable region ("D-Loop 3") of the mitochondrial genome, spanning nps 16210-16330 was amplified and sequenced, and molecular sex determination was attempted, both according to Kemp et al. (*5*).

Mitogenome sequencing (University of Illinois, Urbana-Champaign)

50 µL of the DNA extracted at WSU was sent to the University of Illinois and used to create a genomic library with adapters that contained a unique index. The following modifications were made to the TruSeq DNA Sample Preparation V2 protocol. The DNA extract was not sheared because the DNA was already fragmented due to diagenetic processes. A 1:20 dilution of adapters was used because the DNA concentration in the extract was presumably low. Multiple Ampure Bead XP clean ups were completed in an attempt to remove any adapter-dimmer that may have developed. A PCR amplification of the genomic library was prepped in the ancient DNA laboratory (25 µl reaction with 10 µM primers, 5x PCR Buffer, 10 mM Kapa DNTPs, KapaHiFi polymerase, genomic library) and then transported in a sealed environment to a thermocycler in the contemporary DNA laboratory, across campus. The KapaHiFi polymerase was used to amplify the library, as this enzyme has proof-reading properties similar to other polymerases that limit nucleotide misincorporations resulting from cytosine deamination (*79*). The genomic library was amplified for 15 cycles, and cleaned with the Qiagen MinElute Purification Kit. This number of amplification cycles is based on past experience of creating genomic libraries for ancient samples. The quality of the library was assessed on the Agilent 2100 Bioanalyzer using the High Sensitivity DNA kit. The cleaned library was divided into aliquots of 5 µl each for use in additional amplifications until the final concentration reached 100 ng/µl. A target enrichment of the mitochondrial genome was performed on the amplified library using a Rivia customized target enrichment kit following the Rivia target enrichment protocol. A final post-enrichment amplification was performed for 15 cycles. The post-enrichment-amplified product was quantified using qPCR and submitted to the High-Throughput Sequencing Division of the W.M. Keck Biotechnology Center at the University of Illinois Urbana-Champaign.

Bioinformatics analysis: Raw data from the Illumina HiSeq 2000 platform were analyzed with CASAVA 1.8.2. In order to limit contamination that may have been introduced after the clean room library-building step, any reads that did not exhibit the exact index sequence were discarded. Adapter sequences were trimmed using AdapterRemoval (*80*) with a minimum length of 25. Sequence reads were mapped to the human mitochondrial genome revised Cambridge reference sequence (rCRS; *81*) using the Burrows-Wheeler Aligner (BWA) 0.6.2 (*82*) with

default parameters except for seed length, which was set to 1000. Duplicate reads were filtered based on mapping positions (-rmdup -s) using the SAMtools package 0.1.18 (*83*). SNPs and INDELs were called using the SNVer package 0.4.1 (*84*). SNP quality thresholds were set with a haploid model, a read depth of 20, and base quality of 20.

Independent DNA extraction, amplification, and sequencing (University of Texas at Austin)

An additional 55 mg of the molar was removed and sent to the University of Texas at Austin (UT) for independent, blind verification of the results obtained at WSU. All pre-PCR work at UT was conducted in the UT ancient DNA laboratory, which is in a separate building from the post-PCR/modern DNA laboratory. DNA was extracted following the protocol used at WSU, with an extraction negative control (lacking skeletal material) processed simultaneously. Nucleotide positions (nps) 16011-16382 of the mitochondrial genome were amplified and sequenced following Bolnick et al. (*85*); mutations were identified relative to the rCRS. AmpErase® Uracil-N-Glycosylase (Applied Biosystems) was added to some PCR mixes to eliminate template DNA damaged by deamination (*86*), with conditions adjusted following the manufacturer's protocol. The characteristic marker for mtDNA haplogroup D (- *Alu*I at np 5176) was screened following Bolnick et al. (*85*). Molecular sex determination was attempted using the primers given in Kemp et al. (*5*). Contamination controls, as described by Bolnick et al. (*85*), were followed at all stages of the analysis to prevent and detect contamination from exogenous sources.

aDNA Results

Washington State University

The HN-WSU-1 extract amplified with some success for mtDNA. The results demonstrate that this individual is a member of mtDNA haplogroup D (here confirmed twice by observation of the *Alu*I restriction site loss at np 5176). The mtDNA sequence from the HN-WSU-1 extract spanning nps 16210-16330 exhibits 16223T and 16325C and the sequence spanning 16250-16382 exhibits 16325C and 16362C, mutations that are characteristic of the Native American subclade D1 of haplogroup D. Molecular sex determination was not possible; the amelogenin markers failed to amplify twice. The HN-WSU 2 extract also demonstrated that

this individual is a member of mtDNA haplogroup D through observation of the *Alu*I restriction site loss at np 5176. The mtDNA sequence from HN-WSU-2 spanning nps 16210-16330 exhibits 16223T, 16239C/T, 16256C/T, 16260T and 16325C/T, and the sequence spanning 16250-16382 exhibits 16260T, 16325C, 16357C, and 16362C. The 16325C and 16362C mutations are characteristic of the Native American subclade D1 of haplogroup D. The differences observed between amplicons from the two extractions conducted at WSU may be due to post mortem damage to the DNA strands (i.e., miscoding lesions). The inconsistencies are also consistent with a very low level of DNA preserved in this specimen. It should be noted that no members of the collection team belong to haplogroup D, nor do any members of Kemp Laboratory. Moreover, no evidence of haplogroup D was observed in any of the extraction or PCR negative controls from the experiments at WSU.

University of Illinois, Urbana-Champaign

The sequencing analysis revealed multiple mitogenomes, belonging to haplogroup D1 and a non-D haplogroup, in the genomic library. As the DNA sequence results from WSU exhibited only sequences belonging to haplogroup D1, the additional non-D sequences were likely introduced during genomic library construction.

We identified the non-D1 haplogroup contaminant sequences in two ways. First, for nucleotide positions with derived alleles specific to haplogroup D1, allele counts were generated for the allele consistent with D1 and the alternative allele not consistent with D1. For this analysis the derived specific D1 alleles ranged from 16%-88% of the total count depending on the nucleotide position, with an average of 64% for all nucleotide positions examined. In addition, sequences were parsed into three categories: 1) Sequences that matched haplogroup D1 sequences, 2) Sequences that did not match haplogroup D1 sequences and 3) Indeterminate sequences that did not contain enough information to identify whether it matched haplogroup D1 or not. From these analyses we determined that the non-D1 contaminant sequences belong to a sample that was extracted in the UI lab the same week as the library build for the sample analyzed in this study. It is unlikely that the contaminant DNA was introduced during the DNA extraction process at WSU as the RFLP and Sanger sequencing analyses produced a "clean" result with no traces of contamination.

With the removal of the non-D sequences, we were able to confirm nucleotide position substitutions (compared to the rCRS) present in the genomic library with a 26.8x depth. The Hoyo Negro mitogenome includes the defining mutations for haplogroup D and sub-clade D1 at nps 73, 263, 2092, 4883, 5178, 16223, 16325 and 16362.

University of Texas at Austin

Mitochondrial DNA was successfully extracted from the portion of the Hoyo Negro molar sent to UT for analysis. The HN-UT-1 extract exhibits the *Alu*I restriction site loss at np 5176, confirming that this individual is a member of haplogroup D. The mtDNA sequence for nps 16011-16382 was obtained from multiple independent amplifications of four overlapping fragments, and exhibits 16223T, 16239T, 16260T, 16325C, 16357C, and 16362C. The HN-UT-1 extract therefore exhibits the same mutations as the HN-WSU-2 extract, including the 16223T and 16325C mutations that define the D1 sub-clade of haplogroup D. No members of the Bolnick Laboratory belong to haplogroup D, and the negative controls included in the experiments at UT showed no sign of haplogroup D. Three attempts to make molecular sex determination through amelogenin fragment amplification were unsuccessful.

FIGURES S1-S13

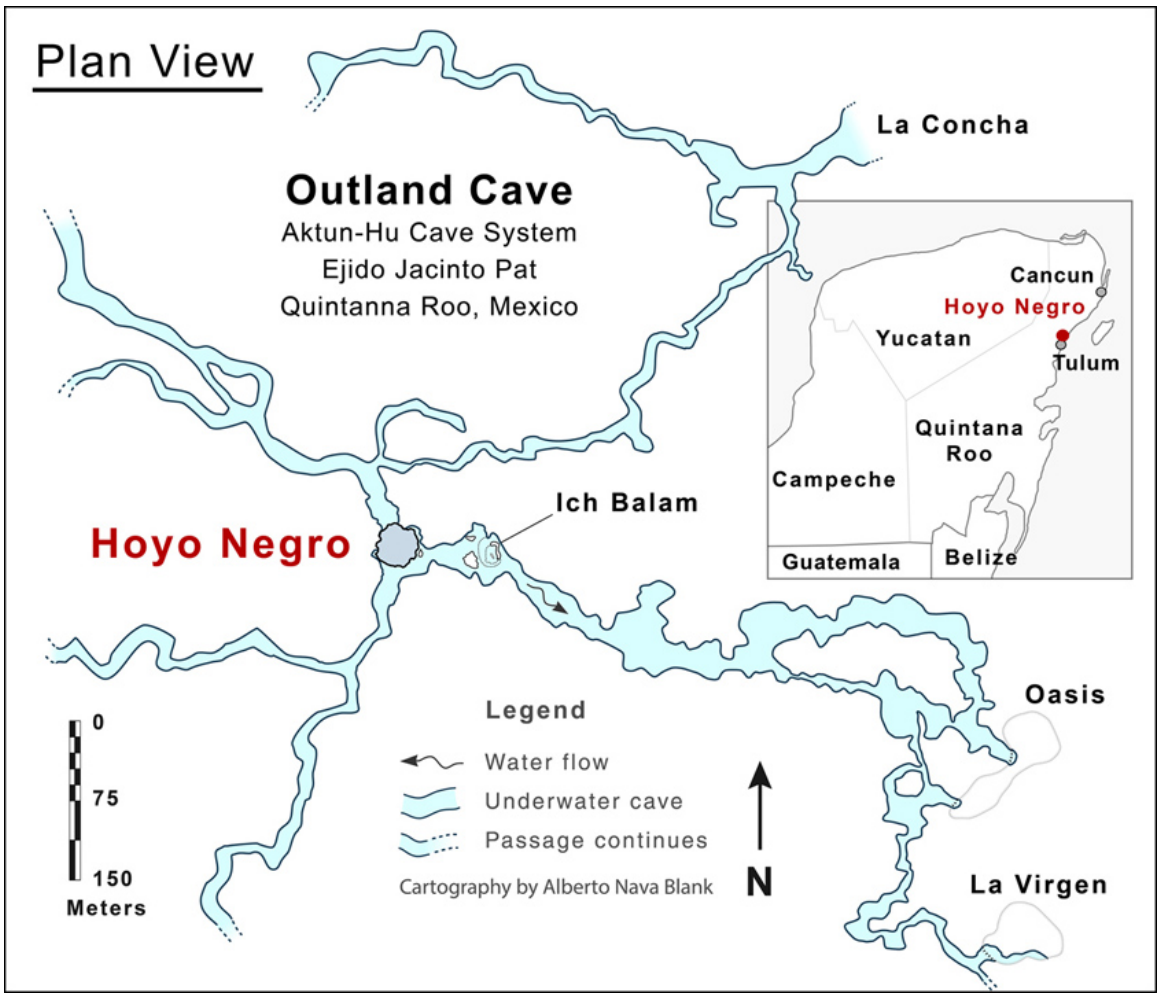

Figure S1. Outland Cave in Quintana Roo State, Mexico, showing Hoyo Negro and its distance from Cenotes La Concha, Oasis, La Virgen and Ich Balam. The passages from HN to Cenotes La Virgen and Oasis have been mapped in detail; only guideline routes have been mapped for the remaining passages. Cartography by Alberto Nava Blank.

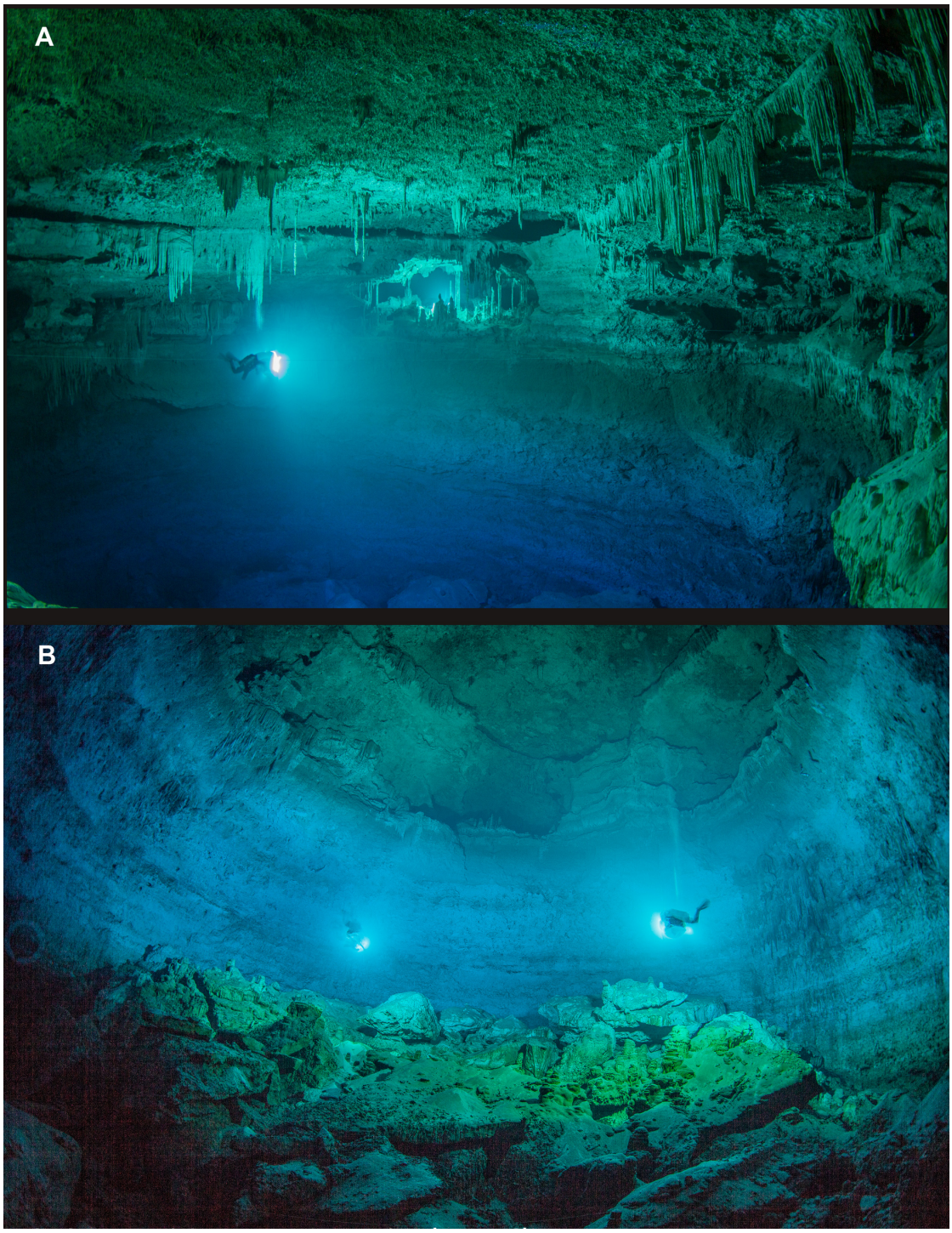

Figure S2. Hoyo Negro seen from the pit rim (A) and from 40 mbsl on the south wall directly below (B). The cascade of stalactites above the diver in (A) is above the remains of the human and *Cuvieronius* 1, located near the small group of flat-topped stalagmites seen on the floor to the left of the left diver in (B). It is the probable source of the mist that formed the florets found on those skeletons. Photos by Roberto Chavez-Arce.

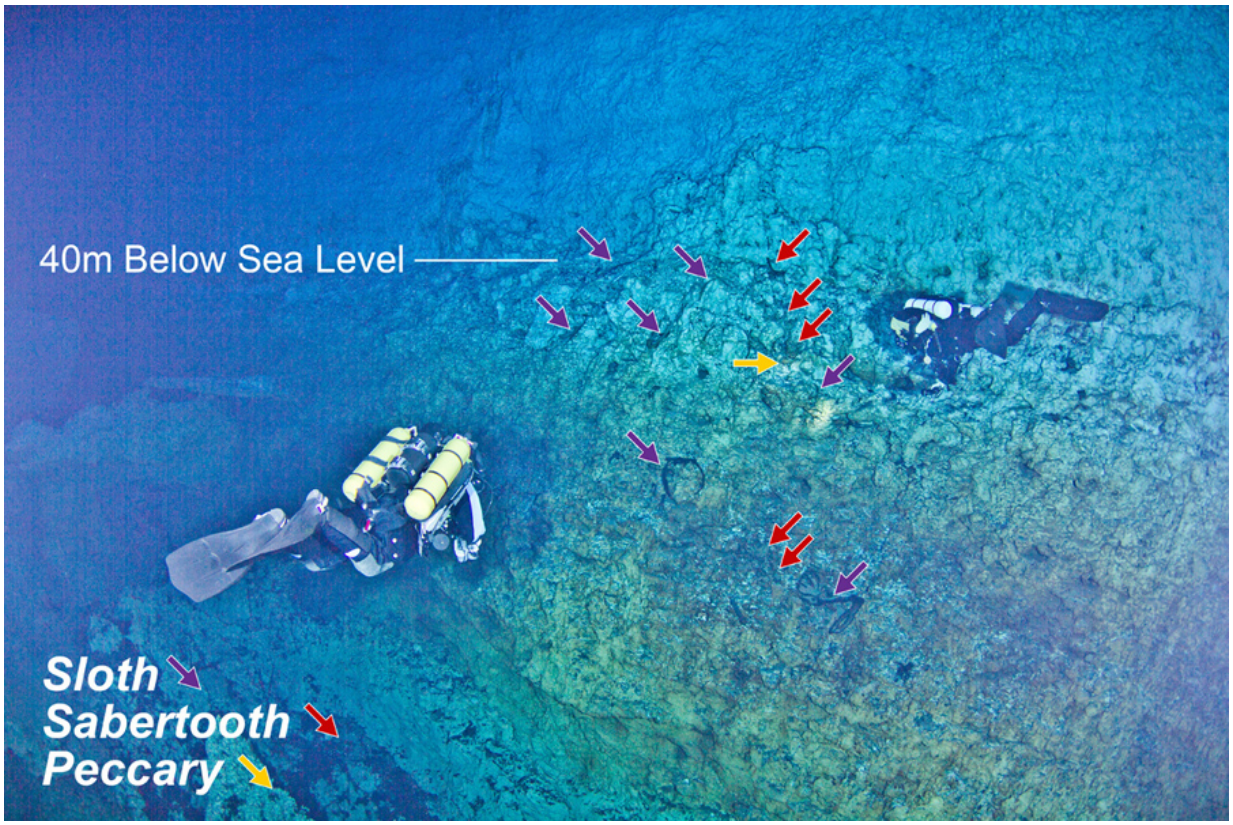

Figure S3. Gray, yellowish-brown and white banding can be seen on this view of a portion of the south wall of Hoyo Negro, showing the scatter of multiple animal skeletons and the broad, iron-stained zone below 41 mbsl. The lowermost black arrow at right marks the *Nothrotheriops shastensis* forelimb seen in Figure S5 (G). Photo by Roberto Chávez-Arce.

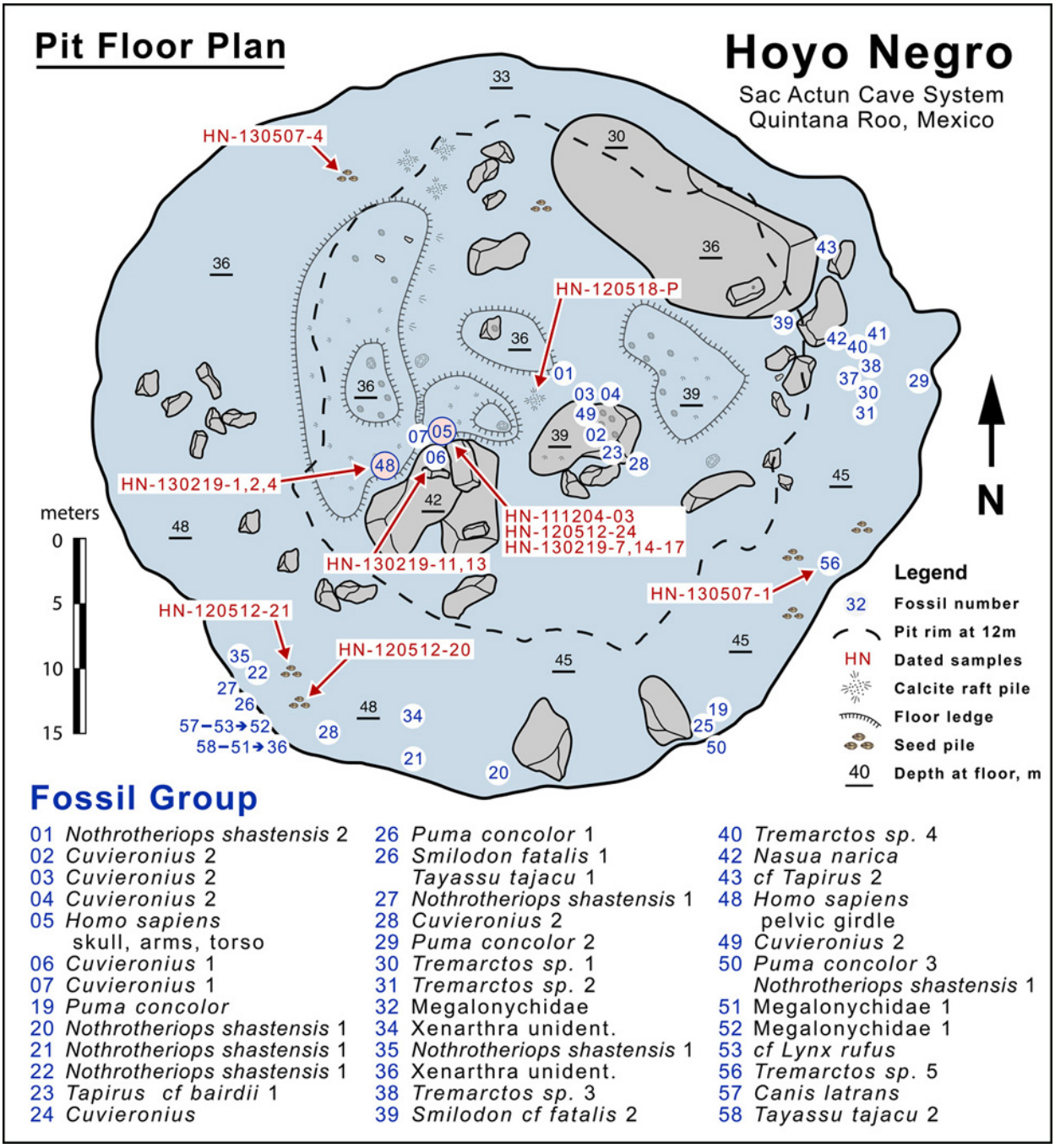

Figure S4. Map of the floor of Hoyo Negro, indicating locations of fossil groups and dated tooth, calcite floret, and seed samples. Skeletal material of human (light red circle) and large mammal bones are distributed in an oval at the deeper southern side of the pit, where their pattern indicates decomposition while floating in water that episodically filled the lower part of the chamber. Cartography by Alberto Nava-Blank.

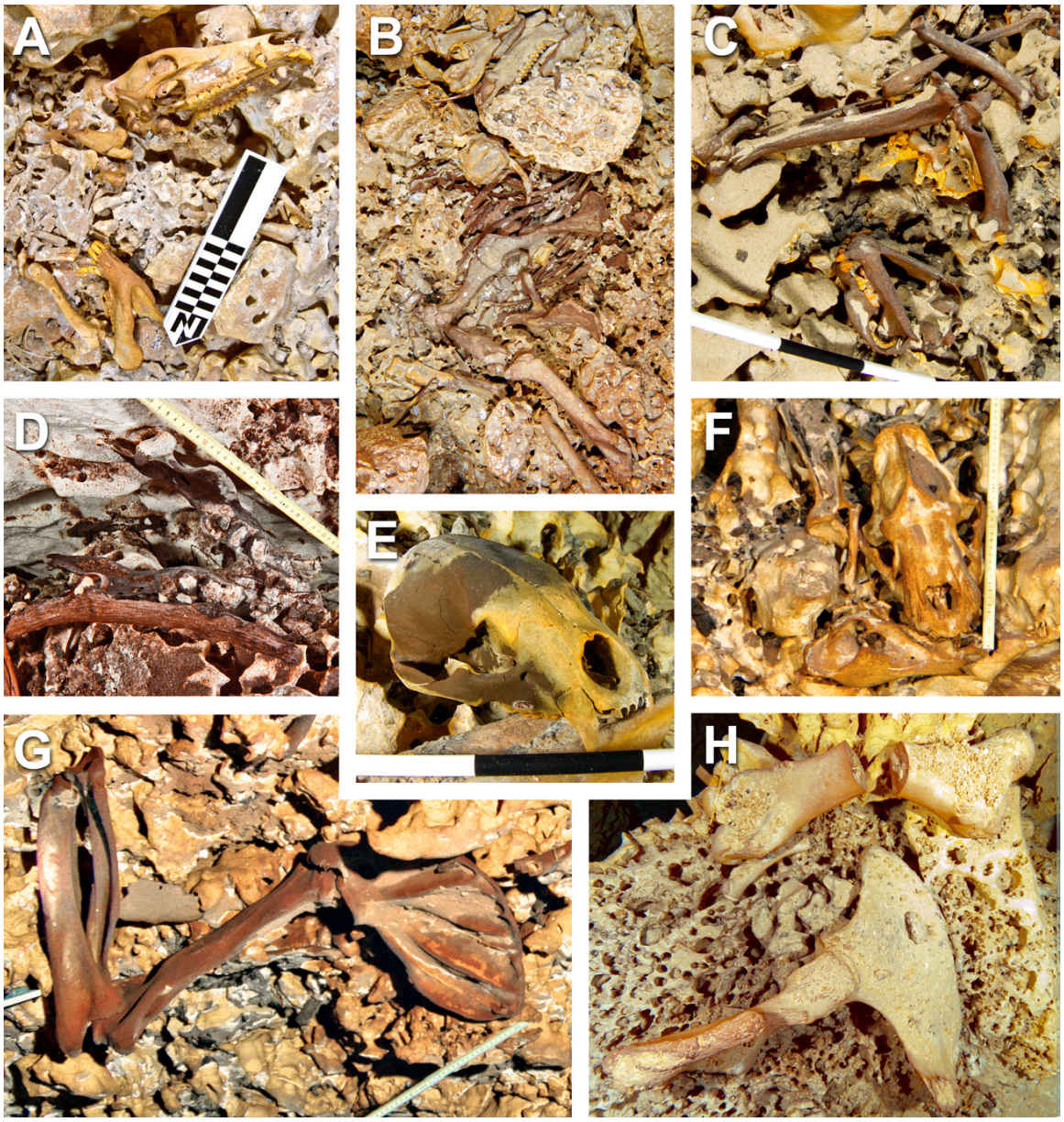

Figure S5. A selection of the large mammals found in Hoyo Negro: *Tayassu pecari* (peccary, A and lower skull in F), *Tapirus cf. bairdii* (tapir, B), *Puma concolor* (cougar, C), a yet-undocumented species of Megalonychid ground sloth (D), Tremarctos sp. (genus including the spectacled bear, E), *Smilodon fatalis* (sabertooth, upper skull in F), *Nothrotheriops shantensis* (Shasta ground sloth, G), and *Cuvieronius cf. tropicus* (highland gomphothere, H). The Megalonychid element is the dentary. The forelimb of *Nothrotheriops*, which is draped on the south wall of the pit near remains of the *Smilodon* and associated *Tayassu* (see Fig. S3) is an example of the process of decomposition that characterizes this deposit. The remainder of this skeleton is distributed across the wall and bottom of the pit, with the articulated synsacrum, femur and lower vertebral column lying on the bottom >5 m to the west (see Fig. S4). All scales are metric. Underwater photos by Roberto Chávez-Arce (A-G) and Daniel Riordan-Araujo (H).

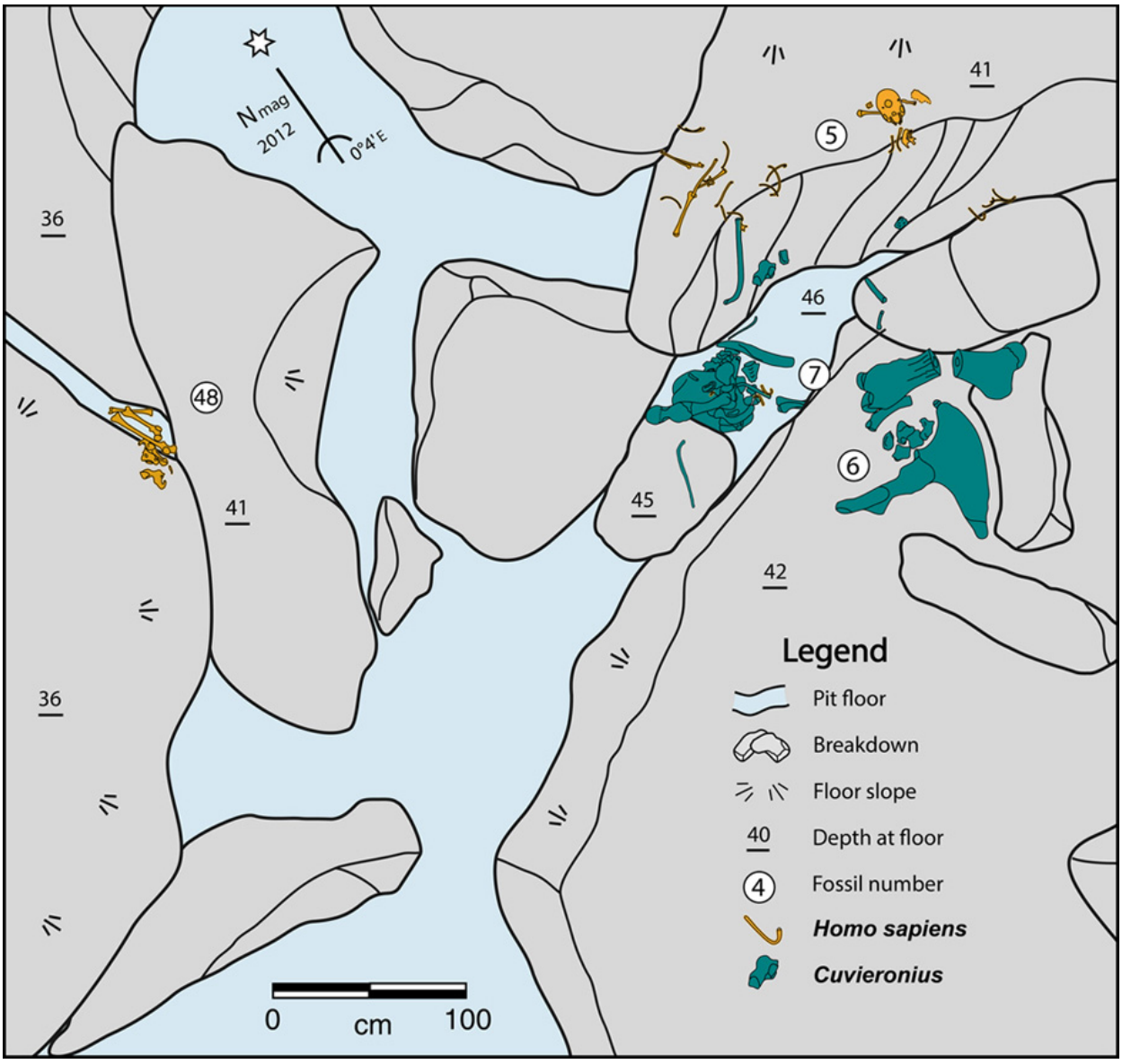

Figure S6. The distribution of human (HN5/48) and gomphothere 1 (*Cuvieronius*; HN-6/7) elements near the center of the HN floor (see Fig. S4). HN5/48 is scattered in four anatomically associated bone clusters: from left to right, the pelvic girdle (group 48); left arm and right forearm with ribs and thoracic vertebrae; skull, mandible, cervical vertebrae the right upper arm, a scapula, a clavicle, and additional ribs; and a cluster of four ribs (group 5). Three additional ribs, horizontally closest to the skull cluster, occur in the adjacent pit on a pile of gomphothere bones (group 7). This pattern of articulated anatomical units scattered in horizontally separate groups is consistent with a body decomposing as a floating corpse.

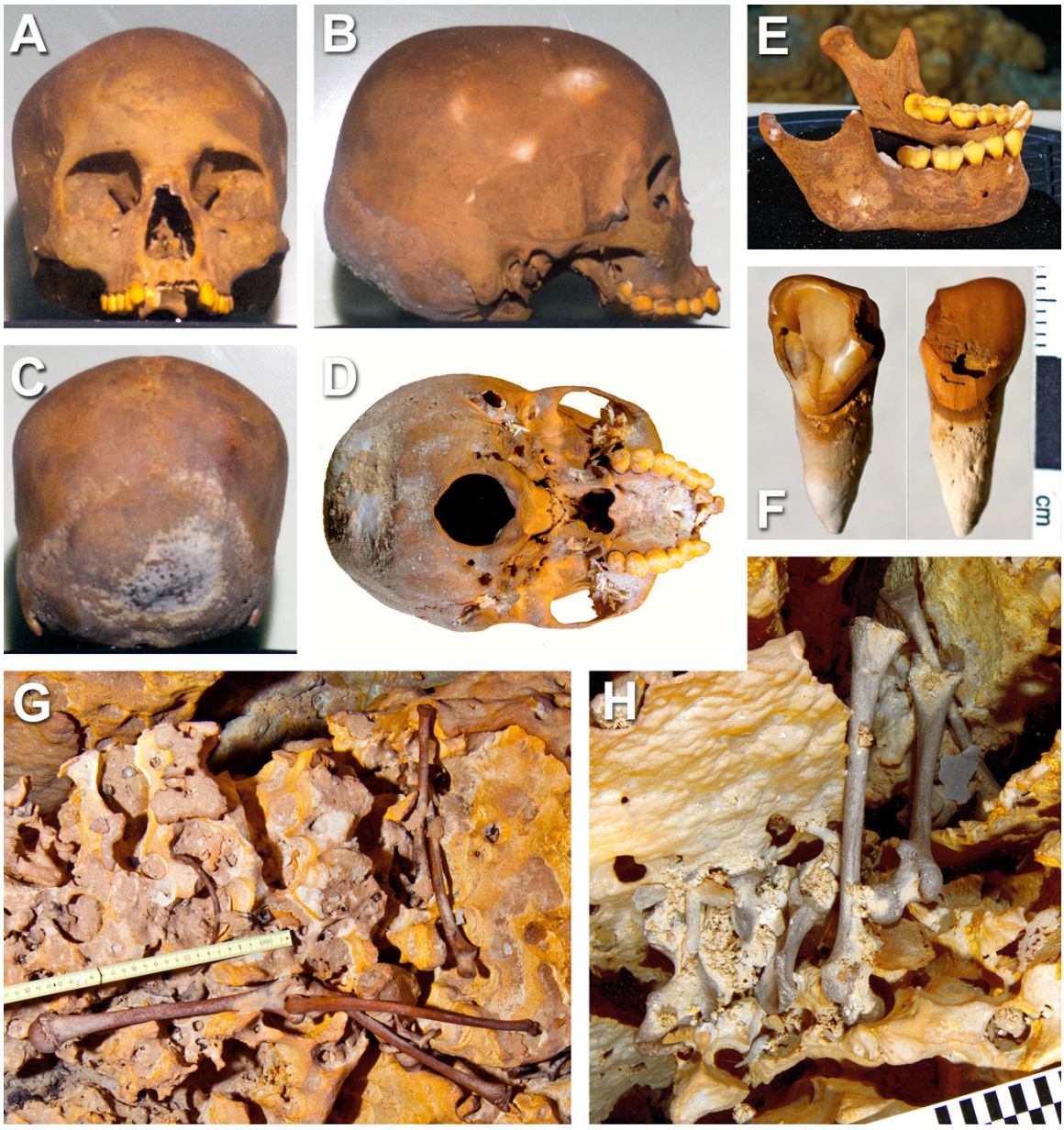

Figure S7. Portions of the human skeleton HN5/48, including the skull (A-E), upper first incisor (F) arms and associated ribs and vertebrae (G) and the pelvic girdle (H). The cranium is shown in anterior (A), left lateral (B), posterior (C) and basal (D) views. Note the lack of projecting zygomatics and the proportionate shortness of the upper face (A, B), the angle formed by the occipital bones (B), and the parabolic dental arcade (D). The upper right third molar (B, D) is fully erupted, whereas the upper left has emerged but is not yet in occlusal position. Lower third molars, however, appear to be impacted. Note the well-developed shoveling and three large carious lesions in F. Scales are metric. All photos except F taken underwater by Roberto Chávez-Arce; (G) and (H) were taken in situ.

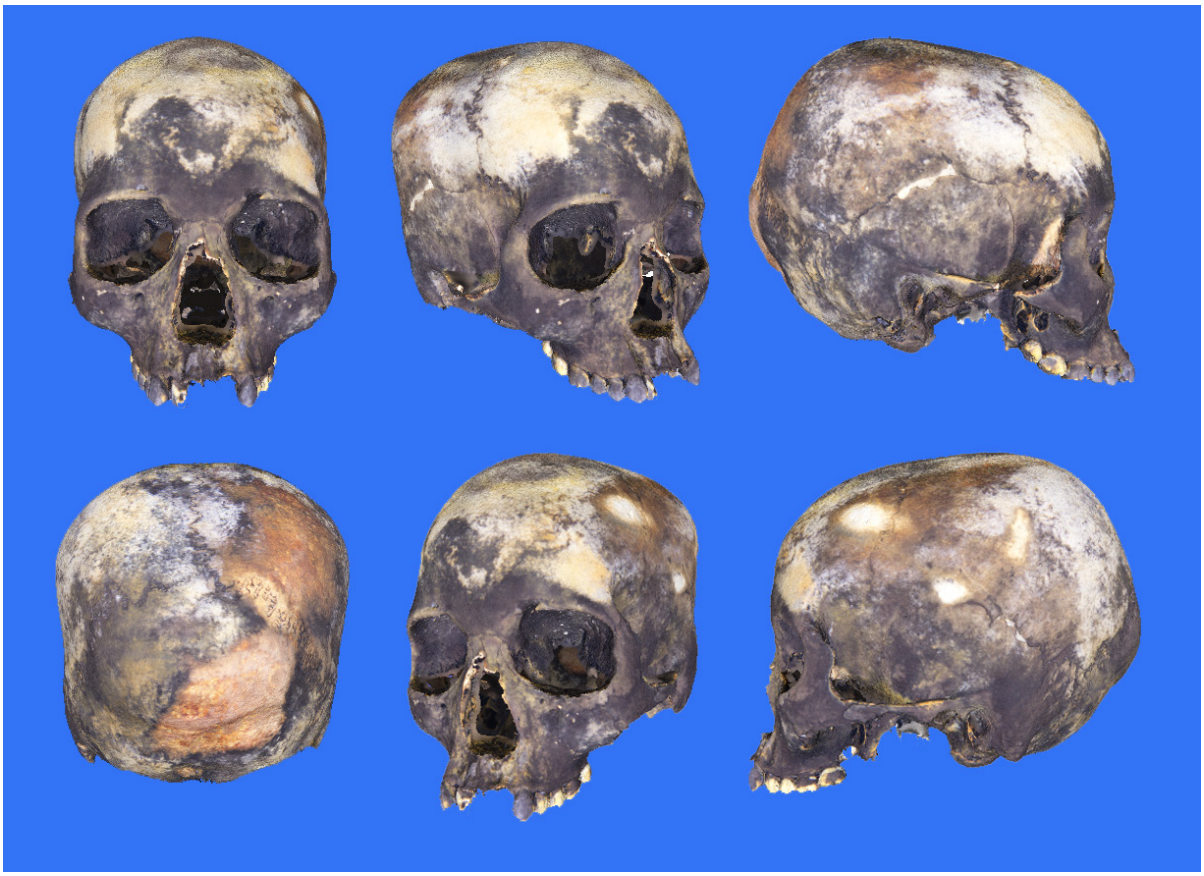

Figure S8. Multiple views of the skull of HN5/48 taken as screen grabs of a digital 3-D model produced from photographs. On screen, the model has a strong parallax effect, which is particularly evident in front and ¾ views. Color here differs from that seen in other figures due to a redox reaction caused by temporary protective underwater storage in a closed vessel. It has since reverted to its original color. Model by Ann Jaskolski and Corey Jaskolski from photos by Roberto Chávez-Arce.

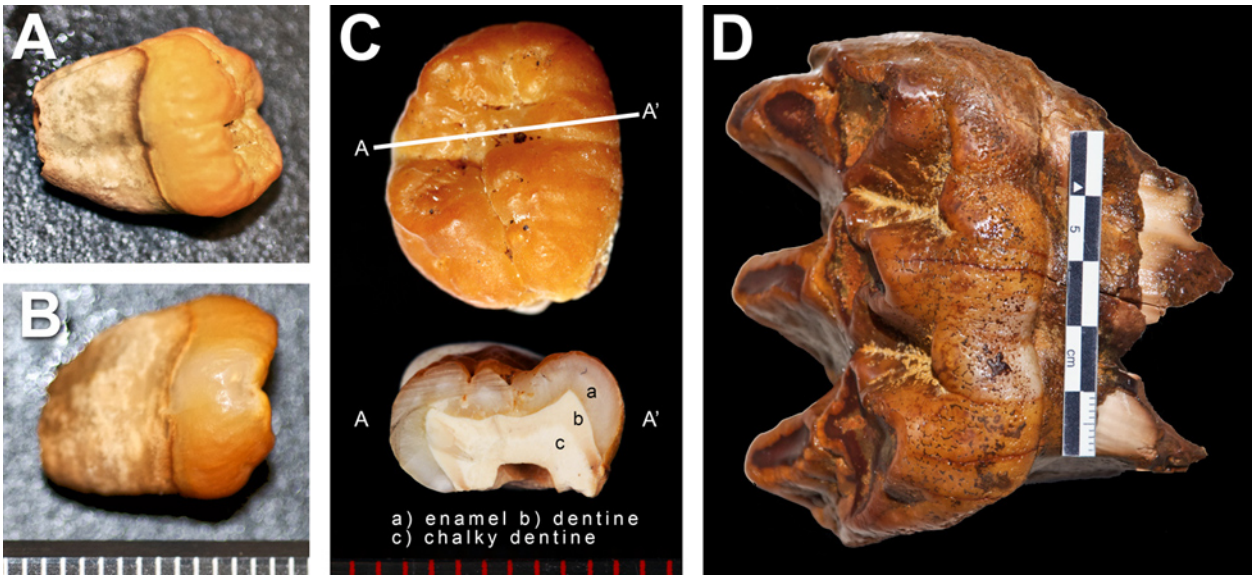

Figure S9. The upper left third molar of HN5/48 (A-C) sampled for ^{14}C and aDNA analysis and the gomphothere molar used for ^{14}C analysis (e). A and B were taken in the ancient genetics laboratory at Washington State University prior to removal of the tooth root for aDNA analysis. Dentine and enamel of both teeth were sampled for ^{14}C measurement.

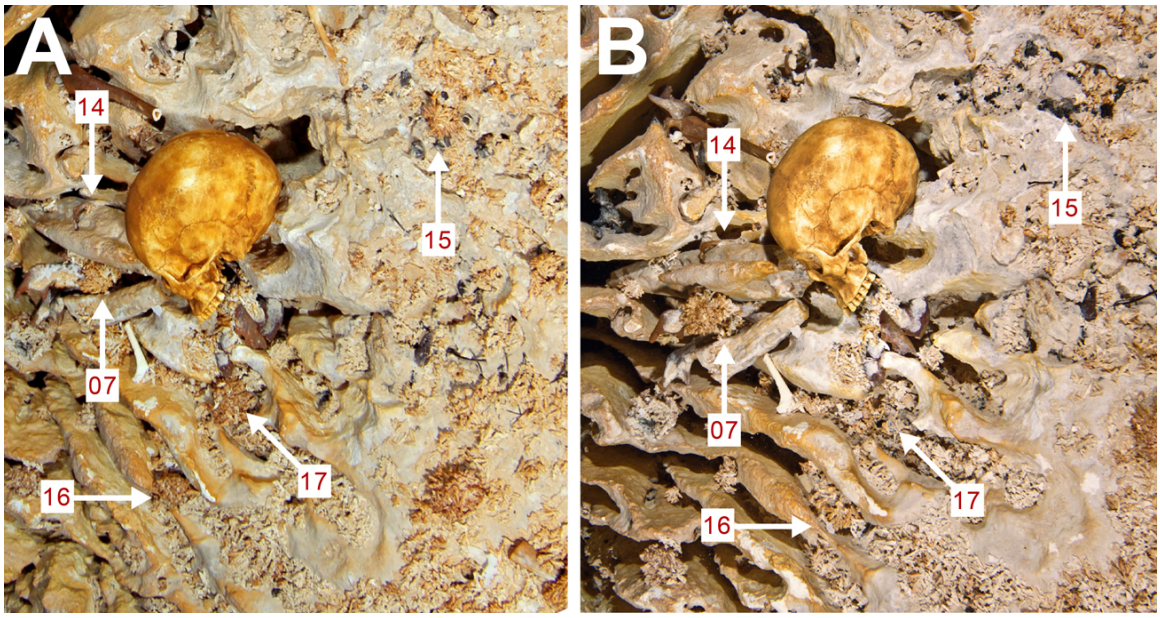

Figure S10. Before (A) and after (B) photos of florets from on and near human bones. Divers entered the site with laminated photos labeled as in A to correctly identify florets selected for sampling. Those on the human bone are 07 (mandible), 14 (rib; see Fig. S11), and 17 (scapula). The floret in the 07 position in B is a replacement positioned to mask the underlying mandible from view by unauthorized visitors. Photos by Roberto Chávez-Arce; the skull in this image is a plastic stand-in lain in the place of the original after unauthorized divers put the original at risk.

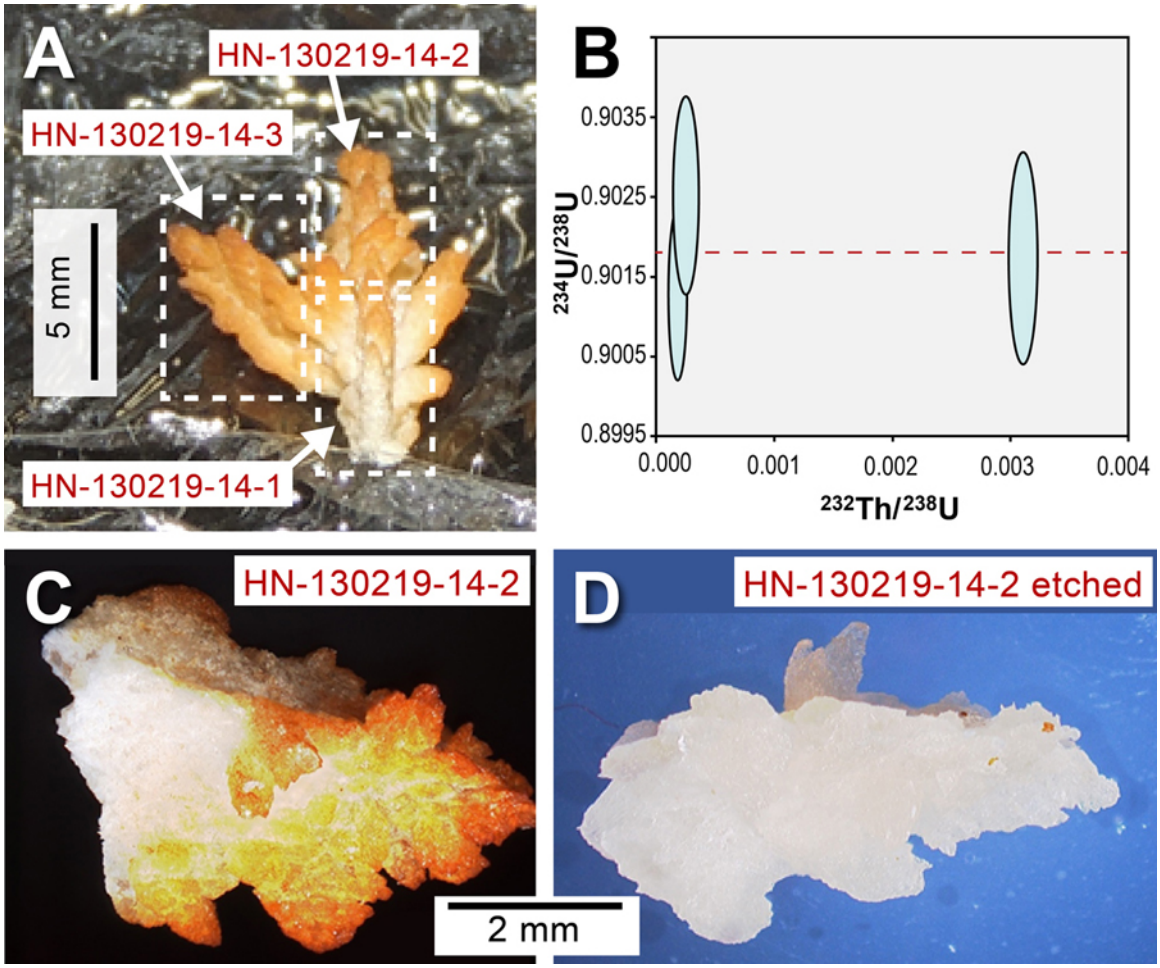

Figure S11. An example of floret processing. Floret HN130219-14 (A) was detached from one of HN5/48's ribs. This small floret branched as two fronds. It was sampled three times, the trunk (1), and the branches (2, 3) for U-Th analyses. This sample consisted of dense calcium carbonate. The floret's dark yellowish-brown stain (A, C) was removed using a procedure described in the supplementary text. The clean sub-samples (D) produced robust and reliable U-Th ages. U-Th analysis of these three sub-samples produced a ^{230}Th-^{234}U-^{238}U isochron age of 11.3 ± 0.6 ka (B). The initial $^{230}Th/^{232}Th_{activity}$ value from this isochron was 5.5 ± 3.0 (atomic ratio = 32 ± 16 ppm), which was used to correct all U-Th ages.

Sample	^{238}U (ppb)	^{232}Th (ppb)	$\delta\,^{234}U_m$	$\delta\,^{234}U_i$	Age (corrected)
FS2 - exp1 etched	913 ± 1	67 ± 84	509 ± 2	531 ± 2	14988 ± 54
FS2 - exp2 not etched	935 ± 1	21 ± 31	507 ± 2	528 ± 2	14758 ± 41
FS2 - exp1 leachate	793 ± 1	183 ± 487	509 ± 2	531 ± 2	14795 ± 171

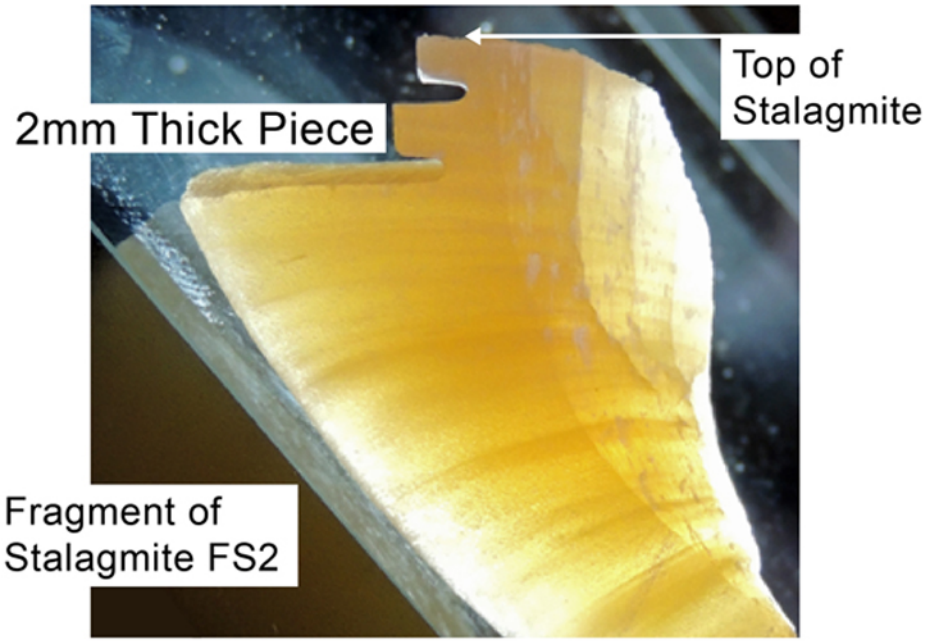

Figure S12. To evaluate the effects of the leaching process, a 2 mm-thick piece was cut from the top of stalagmite FS2 (from Fort Stanton Cave, New Mexico, USA) along a growth layer. The distance from the stalagmite top is equivalent to 11.0-13.5 mm of the FS2 chronology of Polyak *et al.* (*86*). This was selected so that all sub-samples from this piece should have ages of 14.6 to 15.0 ka, which are similar to that of the florets. Stalagmite FS2 also has a uranium concentration similar to that of the florets. FS2-exp1 included three small pieces that were etched in 0.5 M HNO_3 for 60 seconds. 15% of FS2-exp1 was dissolved, and collected as FS2-exp1-leachate. FS2-exp2 was a single sub-sample of the 2mm-thick piece, and was not treated. The results above show that etching with 0.5 M HNO_3 for 60 seconds does not affect the age results within our age limits of 14.6 to 15.0 ka. Corrected ages are years before AD 2011. $\delta^{234}U_m$ = measured value and $\delta^{234}U_i$ = initial value in ‰.

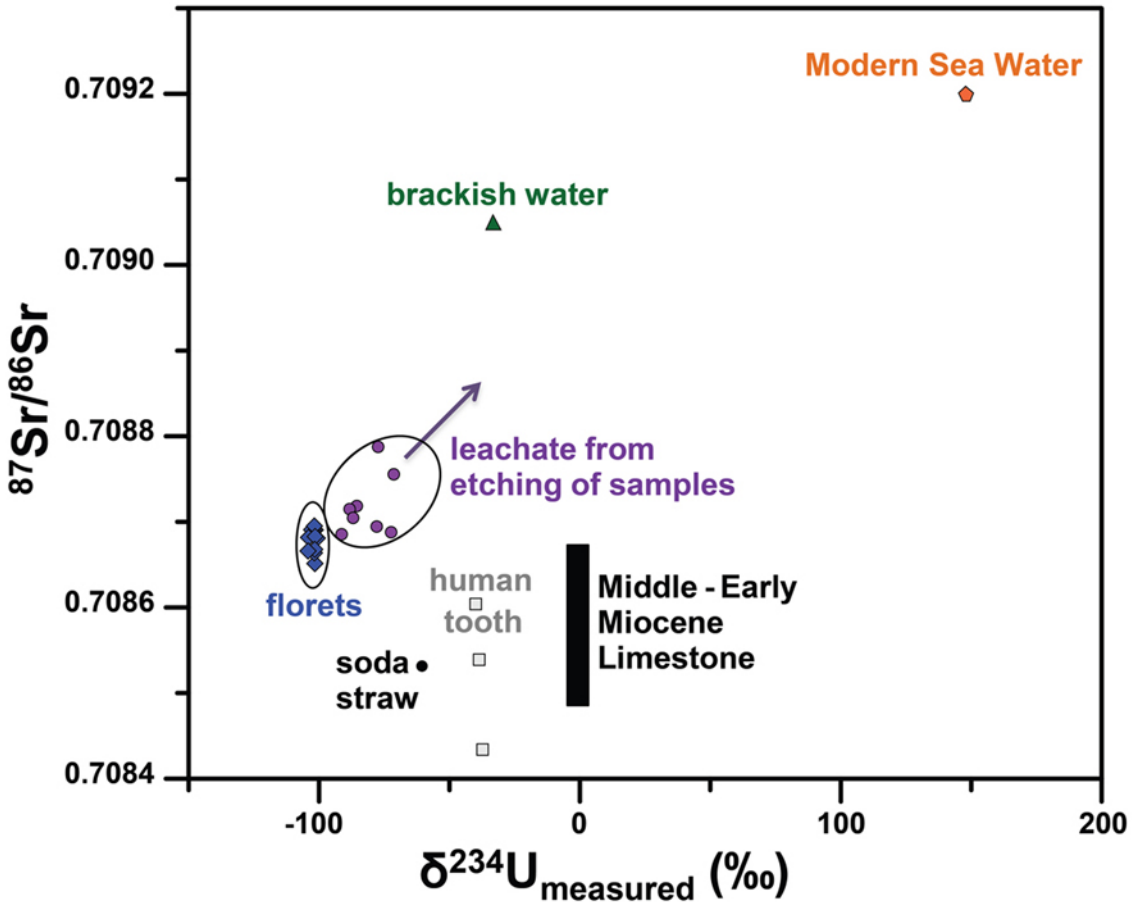

Figure S13. Comparison of $\delta^{234}U$ versus $^{87}Sr/^{86}Sr$ shows that the florets are distinct from marine water (*63*) of brackish water from HN (42 mbsl), while leachate values show that the dark yellowish-brown outer layer of the florets likely formed from contact with marine water or the brackish water from the 40 mbsl level of the pit. The florets, like a fallen soda straw stalactite collected from the rim of HN, and the human tooth have a value similar to middle to early Miocene limestone (*63*). The florets likely formed from drip water or vadose pool waters that had a limestone isotopic composition.

TABLES S1-S5

Table S1. Paleoamerican human skeletons predating ~8800 RC BP (10,000 CAL BP)[1].

Skeleton	Location	^{14}C age, RC yr BP	Dated material	Assemblage, age, sex	Reference
Icehouse Bottom	TN, USA	8800-9300	context	Cremated bone fragments, adult, F	(***87***)
La Brea	CA, USA	9000±80	Bone collagen	Partial skull, postcranial; 16-18, F	(***88, 89***)
Tuqan	CA USA	8965±30	Assoc sediments	Skull, partial longbones, 36-46, M	(***90***)
Spirit Cave Cremation	NV, USA	9040±50	Assoc. textile	Cremated bone fragments, 18-22, F	(***91, 92***)
On Your Knees Cave	AK, USA	9200[2]	Bone collagen	Skeletal fragments, 20-25, M	(***93***)
Wizards Beach	NV, USA	9225±60[*]	Bone collagen	skull and skeletal elements, 32-42, M	(***92***, ***94***)
Guavio I	COL	9360±45	Not reported	…, …, Male	(***95***)
Spirit Cave mummy	NV, USA	9415±25	Hair	Complete skeleton (mummy), 40-44, M	(***92***, ***96***)
Marmes CH I	WA, USA	9430±40, 9360±60	Age of stratum	Cremated bone fragments, mid adult, M	(***97***, ***98***)
Marmes CH II	WA, USA	9430±40, 9360±60	Age of stratum	Cremated bone fragments, adult, I	(***97***, ***98***)
Marmes CH III	WA, USA	9430±40, 9360±60	Age of stratum	Cremated bone fragments, 12-18, M	(***97***, ***98***)
Marmes CH IV	WA, USA	9430±40, 9360±60	Age of stratum	Cremated bone fragments, adult, I	(***97***, ***98***)
Marmes CH V	WA, USA	9430±40, 9360±60	Age of stratum	Cremated bone fragments, ca. 8, I	(***97***, ***98***)
Marmes CH VI	WA, USA	9430±40, 9360±60	Age of stratum	Cremated bone fragments, ca 8, I	(***97***, ***98***)
Grimes Point Cave 1	NV, USA	9470±60	Assoc. (?) fabric	Cranium, 6-8, I	(***91***, ***92***)
Grimes Point Cave 2	NV, USA	9470±60	Assoc. (?) fabric	Postcranial bone fragments, 16-18, M	(***91***, ***92***)
Lauricocha	PERU	>9500	Not reported	11 individuals	(***14***)
Horn Shelter II, no 1	TX, USA	9500±200, 9980±370[3]	Age of stratum	Complete skeleton, 35-45, M	(***99***)
Horn Shelter II, no 2	TX, USA	9500±200, 9980±370[3]	Age of stratum	Complete skeleton, 11-13, F	(***99***)
Wilson-Leonard	TX, USA	9600-10,000	Age of bracketing strata	Crushed skull, partial longbones, 20-25, F	(***72***, ***100***)
Gordon Creek	CO, USA	9700±250	Bone collagen	Complete skeleton, 26-30, F	(***101***)
Marmes I	WA, USA	9710±40, 9870±50	Age of stratum	Cremated fragments, young adult, F	(***97***, ***98***)
Marmes II	WA, USA	9710±40, 9870±50	Age of stratum	Cremated fragments, 6, I	(***97***, ***98***)
Marmes III	WA, USA	9710±40, 9870±50	Age of stratum	Cremated bone fragments, young adult, M	(***97***, ***98***)
Marmes IV	WA, USA	9710±40, 9870±50	Age of stratum	Cremated bone fragments, I	(***97***, ***98***)
Tequendama	COL	9740±135	Not reported	Remains of 5 M, 4 F	(***95***)
Arch Lake	NM, USA	10,020±50[4]	Bone collagen	Complete, deteriorated skeleton, 17-20, F	(***102***)
Tlapacoya I	MX, EUM	10,200±65	Bone collagen	Calotte, 30-35, M	(***103***)
Lapa Vermelha IV	BR	>10,200±220[5]	Associated (?) stratum	Cranium, partial skeleton,	(***14***)

Skeleton	Location	^{14}C age, RC yr BP	Dated material	Assemblage, age, sex	Reference
Buhl	ID, USA	10,675±95	Bone collagen	Skull and skeletal elements, 17-21, F	(***104***)
Anzick (infant)	MT, USA	10,705±35 [6]	Bone collagen	Fragments of skull, rib, clavicle 1.5, I	(***2***)
Peñon III	MX, EUM	10,755±75	Bone collagen	Skull and skeletal elements, 25, F	(***103, 105***)
Arlington Springs	CA, USA	10,960±80	Bone collagen	Two partial femora, patella, adult, M	(***106***)
Hoyo Negro	QR, EUM	10,976±20[6,7]	Tooth enamel	Largely complete skeleton, 15-16, F	This article

1. Fishbone Cave, Warm Mineral Springs not included because of a standard deviation > 250 years and/or lack of a clear association of dated material and skeleton. Naharon is excluded based on Taylor (*45*). 2. Reported marine reservoir corrected age. 3. Included despite high standard deviation (>250) because associated artifacts are consistent with this chronology. 4. Oldest in a date series, believed to represent most suitable chemical fraction. 5. Often claimed to date 11,700 BP (maximum age of presumed associated stratum), Lapa Vermelha IV cannot be securely linked to radiocarbon dates on charcoal in sediment; an age of ca 9000 BP is more likely (*107*). 6. Mean of multiple dates. 7. Possibly contaminated with fossil carbon, this is a maximum age, minimum age based on U-Th analysis is 11,930±181.

Table S2. Large mammal species documented in Hoyo Negro.

Order	Family	Genus/Species	Common Name	MNI	Min. Depth(s)[1] mbsl[1]
Artiodactyla	Tayassuidae	*Tayassu pecari*	Collared peccary	2	41.2, 41.7
Carnivora	Canidae	*Canis latrans*	Coyote	2	41.8
	Felidae	*cf. Lynx rufus*	Bobcat	2	41.0
		Puma concolor	Cougar	3	42.9, 43.0, 44.1
		Smilodon cf. fatalis	Sabertooth	2	39.8
	Procyonidae	*Nasua narica*	White-nose coati	1	…
	Ursidae	*Tremarctos* sp.	Tremarctine bear	6	44.1, 45.3, 46.2, 46.2
Primates	Hominidae	*Homo sapiens*	Human	1	41.6
Perissodactyla	Tapiridae	*Tapirus* sp.	Tapir	2	40.5, 41.7
Proboscidea	Gomphotheridae	*Cuvieronius* sp.	Gomphothere	2	41.9, 42.6
Xenarthra	Nothrotheriidae	*Nothrotheriops shastensis*	Shasta ground sloth	2	41.3, 41.4
	Megalonychidae	Un-named genus/species	Ground sloth	1	40.1

1. Depth of some individuals not yet confirmed.

Table S3. ^{14}C Measurements on human and gomphothere enamel, floret calcite, bat guano, and U-Th ages on florets.

Sample Name	Lab Number	Description	Material	Depth (m)	^{14}C Age, RC yr.	2σ cal BP
Radiocarbon						
HN111204-3	SR-8205 / UCIAMS-119438	Female human upper 3rd molar enamel	Bioapatite	41.6	10,970±25	12,915-12,720
HN111204-3	PSU-5493 / UCIAMS-123541	Female human upper 3rd molar enamel	Bioapatite	41.6	10,985±30	12,965-12,730
HN111204-2	DAMS-4981	Female human rib	Bioapatite	42.3	16,164±78	19,741-19,246
HN120512-20a	DAMS-2599a	Apex of subaqueous bat guano 1, pit floor	Seed	48.0	8925±41	10,200-9910
HN120512-20b	DAMS-2599b	Apex of subaqueous bat guano 1, pit floor	Seed	48.0	8823±48	10,155-9980 (28.6%) 9970-9690 (66.8%)
HN120512-21	DAMS-2600	Apex of subaqueous bat guano 2, pit floor	Seed	48.0	8605±45	9685-9515 (94.9%) 9510-9500 (0.5%)
HN130513-1	DAMS-3373	Apex of subaqueous bat guano 3, pit floor	Seed	48.3	8074±37	9125-8950 (79.7%) 8920-8860 (7.1%) 8835-8780 (8.7%)
HN130513-3	DAMS-3374	Apex of bat guano 4, pit floor	Seed	37.1	8666±38	9700-9540
HN130513-4	DAMS-3375	Subaqueous bat guano overlying Tremarctos HN56	Seed	46.1	9565±37	11,095-10,735
HN120518-P.S1	Beta-333189	Surface of shallow subaqueous bat guano, pit floor	Seed	42.0	8620±50	9700-9515
HN120518-P.S2	DAMS-3404	Surface of shallow subaqueous bat guano, pit floor	Seed	42.0	8826±31	10,150-10,060 (17.9%) 10,040-10,020 (1.6%) 10,015-9985 (3.0%) 9955-9700 (72.8%)
HN120512-24	SR-8206 / UCIAMS-119439	Cuvieronius molariform, enamel	Bioapatite	41.9	36,250±370	41,610-40,075
HN120512-24	PSU-5493 / UCIAMS-123542	Cuvieronius molariform, enamel	Bioapatite	41.9	33,190±370	38,405-36,400
Uranium-Thorium						
HN130219-7.6	HN-7-6	Floret from human mandible (frond 6)	Calcite	41.9		10,888±213
HN130219-7.7	HN-7-7	Floret from human mandible (frond 7)	Calcite	41.9		10,462±237
HN130219-14.2	HN-14-2	Floret from human rib (frond 2)	Calcite	41.9		11,106±112
HN130219-14.3	HN-14-3	Floret from human rib (frond 3)	Calcite	41.9		11,418±146
HN130219-17.1a	HN-17-1a	Floret from human scapula (frond 1)	Calcite	41.7		11,192±140

Sample Name	Lab Number	Description	Material	Depth (m)	^{14}C Age, RC yr.	2σ cal BP
HN130219-17.2a	HN-17-2a	Floret from human scapula (frond 2)	Calcite	41.7		11,930±181
HN130219-17.4a-A	HN-17-4a-A	Floret from human scapula (frond 4, run 1)	Calcite	41.7		9504±71
HN130219-17.4a-B	HN-17-4a-B	Floret from human scapula (frond 4, run 2)	Calcite	41.7		9843±80
HN130219-17.5a	HN-17-5a	Floret from human scapula (frond 5)	Calcite	41.7		10,965±105
HN130219-11-1	HN-11-1	Floret from Cuvieronius 1 innominate	Calcite	42.6		13,572±320
HN130219-11-2	HN-11-2	Floret from Cuvieronius 1 innominate	Calcite	42.6		15,073±178
HN130219-11-3	HN-11-3	Floret from Cuvieronius 1 innominate	Calcite	42.6		18,823±256
HN130219-13-1	HN-13-1	Floret from Cuvieronius 1 innominate	Calcite	42.7		16,413±167
HN130219-13-3	HN-13-3	Floret from Cuvieronius 1 innominate	Calcite	42.7		11,872±266

Table S4. Uranium-series (U-Th) data for 'floret' speleothems from Hoyo Negro, Mexico.

Sample	^{238}U (ppb)	^{232}Th (ppt)	$^{230}Th/^{232}Th$	$^{230}Th/^{238}U$	$\delta^{234}U_m$	$\delta^{234}U_i$	Uncorrected Age (yrs BP)	Corrected Age (yrs BP)	$^{87}Sr/^{86}Sr$
Analyses of pieces of florets on human bones									
HN-7-6*	1221 ± 1	2347 ± 92	142 ± 6	0.0895 ± 0.0004	-98 ± 1	-101 ± 1	11,404 ± 53	10,888 ± 233	
HN-7-7*	1261 ± 1	2480 ± 66	134 ± 4	0.0863 ± 0.0003	-99 ± 1	-102 ± 1	10,989 ± 45	10,462 ± 237	
HN-14-2*	1149 ± 1	602 ± 228	517 ± 196	0.0885 ± 0.0006	-99 ± 1	-102 ± 1	11,292 ± 81	11,106 ± 112	0.70869
HN-14-3*	1058 ± 1	783 ± 280	377 ± 135	0.0913 ± 0.0007	-98 ± 1	-101 ± 1	11,655 ± 100	11,418 ± 146	0.70868
HN-17-1a*	1061 ± 1	1172 ± 97	249 ± 21	0.0902 ± 0.0003	-99 ± 1	-104 ± 1	11,516 ± 47	11,192 ± 140	
HN-17-2a*	1023 ± 1	1512 ± 85	199 ± 11	0.0963 ± 0.0003	-98 ± 1	-102 ± 1	12,342 ± 47	11,930 ± 181	
HN-17-4a-A*	1188 ± 1	599 ± 66	463 ± 51	0.0764 ± 0.0003	-100 ± 1	-102 ± 1	9686 ± 36	9504 ± 71	0.70869
HN-17-4a-B*	1091 ± 1	642 ± 52	411 ± 33	0.0791 ± 0.0003	-100 ± 1	-103 ± 1	10,045 ± 37	9843 ± 80	0.70869
HN-17-5a*	1343 ± 2	1010 ± 92	358 ± 32	0.0880 ± 0.0004	-98 ± 1	-101 ± 1	11,205 ± 54	10,965 ± 105	
Analyses of pieces of floret collected near but not on the human skull and mandible									
HN-15-3*	1177 ± 2	569 ± 46	514 ± 42	0.0812 ± 0.0003	-99 ± 1	-102 ± 1	10,305 ± 44	10,128 ± 72	0.70865
HN-15-4*	1056 ± 3	374 ± 40	676 ± 72	0.0784 ± 0.0003	-99 ± 1	-102 ± 1	9938 ± 43	9792 ± 61	0.70866
HN-16-1*	1132 ± 5	699 ± 46	445 ± 29	0.0900 ± 0.0004	-101 ±1	-104 ± 1	11,515 ± 61	11,306 ± 95	0.70868
HN-16-2*	1109 ± 3	636 ± 89	449 ± 63	0.0862 ± 0.0004	-99 ± 1	-102 ± 1	10,396 ± 45	10,747 ± 100	0.70870
HN-16-3*	1141 ± 2	636 ± 89	449 ± 63	0.0818 ± 0.0003	-99 ± 1	-102 ± 1	10,396 ± 45	10,201 ± 82	0.70868
HN-16-4*	1131 ± 5	1016 ± 74	301 ± 22	0.0883 ± 0.0007	-99 ± 1	-102 ± 1	11,263 ± 95	10,988 ± 143	0.70867
Analyses of pieces of florets on gomphothere bones									
HN-11-1*	1061 ± 1	2807 ± 102	128 ± 5	0.1105 ± 0.0005	-96 ± 1	-100 ± 1	14,260 ± 67	13,572 ± 320	0.708721
HN-11-2*	988 ± 1	1410 ± 87	255 ± 16	0.1192 ± 0.0004	-97 ± 1	-101 ± 1	15,473 ± 54	15,073 ± 178	
HN-11-3*	1044 ± 1	2162 ± 136	216 ± 14	0.1465 ± 0.0005	-97 ± 1	-103 ± 1	19,375 ± 71	18,823 ± 256	

Sample	^{238}U (ppb)	^{232}Th (ppt)	$^{230}Th/^{232}Th$	$^{230}Th/^{238}U$	$\delta^{234}U_m$	$\delta^{234}U_i$	UncorrectedAge (yrs BP)	Corrected Age (yrs BP)	$^{87}Sr/^{86}Sr$
HN-13-1*	1210 ± 1	1547 ± 95	307 ± 19	0.1285 ± 0.0005	-97 ± 1	-102 ± 1	16,778 ± 70	16,413 ± 167	0.708728
HN-13-3*	929 ± 1	2035 ± 114	135 ± 8	0.0971 ± 0.0004	-98 ± 1	-102 ± 1	12,453 ± 56	11,872 ± 266	

yrs BP = years before AD 1950. Corrected ages use an initial $^{230}Th/^{232}Th$ atomic ratio = 32 ± 16 ppm based on a ^{230}Th-^{234}U-^{238}U isochron (*60*) using sub-samples HN-14-1, 2, & 3 (see Fig. S11). * indicates that samples were etched prior to analyses and have <3000 ppb of ^{232}Th. Years before present = yrs BP, where present is AD 2013. All errors are absolute 2σ. All sample names have the prefix 130219, which indicates the collection date of 02-19-2013 (for example, HN-7-6* = HN130219-7-6 etched). Sample weights varied between 20 and 150 mg. All uranium and thorium ratios are activity ratios. m = measured and I = initial, for $\delta^{234}U_m$ and $\delta^{234}U_m$. Absolute errors on $^{87}Sr/^{86}Sr$ ratios are 0.00001 (2σ.).

Table S5: Supplementary uranium-series (U-Th) data for samples from Hoyo Negro, Mexico.

Sample	^{238}U (ppb)	^{232}Th (ppt)	$^{230}Th/^{232}Th$	$^{230}Th/^{238}U$	$\delta^{234}U_m$	$\delta^{234}U_i$	Uncorrected Age (yrs BP)	Corrected Age (yrs BP)	$^{87}Sr/^{86}Sr$
Analyses of untreated pieces of floret									
HN-7middle1	1099 ± 1	6562 ± 161	61 ± 2	0.1200 ± 0.0006	-98 ± 1	-102 ± 1	15602 ± 81	14123 ± 711	
HN-7middle2	1172 ± 7	7433 ± 115	60 ± 1	0.1238 ± 0.0009	-95 ± 1	-99 ± 1	16086 ± 123	14522 ± 757	
HN-7middle3	1331 ± 2	12401± 548	41 ± 2	0.1254 ± 0.0011	-96 ± 1	-100 ± 1	16336 ± 161	14058 ± 1117	
HN-7mid-top4	1389 ± 1	7738 ± 251	66 ± 2	0.1203 ± 0.0006	-97 ± 1	-100 ± 1	15634 ± 83	14334 ± 685	
Analysis of brackish water from collection site									
HN-brackish-water	16 ± 0	17 ± 0	747 ± 13	0.2686 ± 0.0006	-30± 1	-33 ± 1	35408 ± 99	35105 ± 156	0.70905
Analyses of leachates (that contain yellowish-orange stain) from acid etching									
HN-7-5-leachate	1424 ± 7	51623 ± 751	54 ± 1	0.6447 ± 0.0039	-86 ± 1		137497 ± 1784	128297 ± 4761	0.70872
HN-14-1-leachate	806 ± 2	477 ± 1135	338 ± 803	0.0654 ± 0.0035	-91 ± 2		8150 ± 460	7948 ± 570	0.70869
HN-14-2-leachate	1699 ± 4	2016 ± 1004	214 ± 107	0.0832 ± 0.0017	-88 ± 1		10451 ± 219	10112 ± 293	0.70871
HN-14-3-leachate	2462 ± 8	6171 ± 1512	153 ± 38	0.1259 ± 0.0018	-87 ± 1		16213 ± 254	15565 ± 412	0.71087
HN-15-1-leachate	1766 ± 9	13369 ± 2325	110 ± 19	0.2717 ± 0.0055	-71 ± 2		37927 ± 930	36110 ± 1301	0.70876
HN-15-2-leachate	4977 ± 25	48102 ± 2337	83 ± 4	0.2610 ± 0.0028	-72 ± 1		36193 ± 467	33884 ± 1211	0.70869
HN-17-1a-leachate	1281 ± 12	12201 ± 2329	82 ± 16	0.2563 ± 0.0063	-77 ± 2		35650 ± 1057	33361 ± 1572	0.70879
HN-17-2a-leachate	1699 ± 9	14974 ± 2322	73 ± 11	0.2114 ± 0.0040	-78 ± 2		28496 ± 619	26377 ± 1231	0.70869
Analyses of human tooth									
HN-tooth dentine I-1	115984 ± 453	2706 ± 1785	13452 ± 8873	0.1027 ± 0.0006	-36 ± 1	-37 ± 1	12289 ± 77	12221 ± 77	0.70843
HN-tooth dentine I-2	123495 ± 247	1221 ± 874	38996 ± 27913	0.1262 ± 0.0007	-37 ± 1	-39 ± 1	15328 ± 98	15263 ± 98	0.70854
HN-tooth dentine I-3	112906 ± 2510	37 ± 10313	891146 ± 2.506E+08	0.0947 ± 0.0030	-36 ± 1	-37 ± 1	11276 ± 376	11213 ± 377	

Sample	^{238}U (ppb)	^{232}Th (ppt)	$^{230}Th/^{232}Th$	$^{230}Th/^{238}U$	$\delta^{234}U_m$	$\delta^{234}U_i$	Uncorrected Age (yrs BP)	Corrected Age (yrs BP)	$^{87}Sr/^{86}Sr$
Analysis of a soda straw stalactite collected from the ceiling of Hoyo Negro									
HN-18-soda1	1238 ± 2	1210 ± 228	2022 ± 381	0.6466 ± 0.0027	-43 ± 2	-61 ± 2	124312 ± 1086	124029 ± 1089	0.70853
Analyses of samples having yellowish-orange stain, or etched but not cleaned sufficiently – used to set up sample processing procedure									
HN-1-1**	1187 ± 1	2851 ± 168	209 ± 12	0.1640 ± 0.0005	-99 ± 1	-105 ± 1	21981 ± 84	21348 ± 298	
HN-2-1**	1109 ± 1	2424 ± 98	208 ± 8	0.1490 ± 0.0004	-100 ± 1	-105 ± 1	19786 ± 62	19205 ± 267	
HN-4-1**	1091 ± 1	3425 ± 128	123 ± 5	0.1261 ± 0.0005	-98 ± 1	-103 ± 1	16461 ± 66	15656 ± 378	
HN-7-5**	1098 ± 1	3447 ± 175	120 ± 6	0.1232 ± 0.0012	-100 ± 1	-104 ± 1	16096 ± 170	15288 ± 410	0.70867
HN-7-8*	1159 ± 2	4069 ± 716	84 ± 15	0.0962 ± 0.0016	-98 ± 1	-101 ± 1	12316 ± 223	11423 ± 492	
HN-13-2*	1088 ± 1	5309 ± 88	106 ± 2	0.1699 ± 0.0004	-98 ± 1	-104 ± 1	22830 ± 69	21608 ± 582	
HN-14-1*	1177 ± 1	11138 ± 369	34 ± 1	0.1054 ± 0.0009	-98 ± 1	-101 ± 1	13580 ± 127	11264 ± 1130	0.70869
HN-15-1**	1106 ± 1	1088 ± 75	329 ± 23	0.1059 ± 0.0003	-99 ± 1	-101 ± 1	13657 ± 48	13362 ± 126	
HN-15-2**	1041 ± 1	3013 ± 40	169 ± 2	0.1596 ± 0.0004	-98 ± 1	-103 ± 1	21319 ± 64	20570 ± 348	
HN-17-1blue	1092 ± 3	10161 ± 209	75 ± 2	0.2297 ± 0.0010	-95 ± 1	-102 ± 1	32111 ± 170	29828 ± 1117	
HN-tooth enamel/stain	132202 ± 181	42003 ± 490	2380 ± 28	0.2474 ± 0.0008	-40 ± 1		32565 ± 122	32431 ± 127	0.70860

yrs BP = years before AD 1950. All errors are absolute 2σ. Subsample sizes range from 0.5 to 120 mg. Untreated samples produced anomalously high ages. The florets have a yellowish-orange film probably associated with a thin corroded outer layer. Results of the analyses of leachates from etched samples shows that this corroded yellowish-orange layer contains extra ^{232}Th that contributes extra ^{230}Th and causes anomalously high floret ages. Similar results are shown in the analysis of a sample of brackish water from Hoyo Negro. Analyses of the dentine of a tooth from HN5/48 do not produce consistent results, but show apparent ages that are similar to our reported age for HN5/48. All uranium and thorium ratios are activity ratios. m = measured and I = initial, for $\delta^{234}U_m$ and $\delta^{234}U_m$. ** are etched samples used to set up pre-treatment methods. Strontium isotope analyses are relative to standard NMB-987, which has a value of 0.71025, and the absolute error on these ratios is 1E-5 (2σ).

ACKNOWLEDGEMENTS

Research at Hoyo Negro was conducted under permit from the Consejo de Arqueología, Instituto Nacional de Antropología e Historia (INAH), through INAH's Subdirección de Arqueología Subacuática and Centro INAH Quintana Roo. We particularly thank Nelly Margarita Robles García, Pedro Francisco Sánchez Nava, María de los Ángeles Olay Barrientos, Adriana Velázquez Morlet. Funding for this research was provided by the Expeditions Council of the National Geographic Society, the Archaeological Institute of America, the Waitt Institute, INAH, National Science Foundation, Pennsylvania State University, the University of New Mexico, the University of Texas at Austin, and DirectAMS. Project Co-Directors who are not among the authors are Luis Alberto Martos López, Helena Barba Meinecke, and Roberto Chávez-Arce. We owe the utmost gratitude to our scientific divers and surveyors: Alejandro Alvarez, Franco Attolini, Samuel S. Meacham, Gideon Liew, Jacob Mellor, Daniel Riordan-Araujo, Fred Devos, and Christophe Le Maillot. Researchers and engineers who were involved in the project but are not listed among the authors are Shawn Kovacs, Olmo Torres-Talamante, Fabio Esteban Amador, Corey Jaskolski, Ann Jaskolski, Michael Shepard, Eric Berkenpas, Emiliano Monroy Ríos, and James Coke. Shawn Collins provided particular assistance by sharing his initial findings about microfossils in the HN sediment with us. Thanks also to Cara Monroe for conducting the mtDNA typing of the team responsible for collecting the human tooth specimens. Other individuals who acted in supporting capacities are Joaquín García-Bárcena, Christopher Underwood, Tom Deméré, Mark Bauman, O'Shannon Burns, Rebecca Martin, and Terry Garcia. Associated organization and companies are Bay Area Underwater Explorers, Zero Gravity Dive Center, Acuatic Tulum, ProTec, Dive Center Tulum, Quintana Roo Speleological Survey, Rio Secreto, and Centro Investigador del Aquífero de Quintana Roo.

Technical diver Susan Bird conducted all manipulation and collection of human bone and associated florets. Roberto Chávez Arce produced most of the underwater photographs that are presented in online portions of this article. Edward Mallon ably produced or polished most illustrations for this article, including Figures 1 and 3, which were designed by Thomas Harper. Rusty van Rossman produced the drawing of the cranium in Fig 3. Ann and Corey Jaskolski spent many hours manipulating software to produce the 3-dimensional image we used to measure the HN5/48 cranium.

References

1. E. T. Tamm, T. Kivisild, M. Reidla, M. Metspalu, D. G. Smith, C. J. Mulligan, C. M. Bravi, O. Rickards, C. Martinez-Labarga, E. K. Khusnutdinova, S. A. Fedorova, M. V. Golubenko, V. A. Stepanov, M. A. Gubina, S. I. Zhadanov, L. P. Ossipova, L. Damba, M. I. Voevoda, J. E. Dipierri, R. Villems, R. S. Malhi, Beringian standstill and spread of Native American founders. *PLOS ONE* **2**, e829 (2007). doi:10.1371/journal.pone.0000829 Medline

2. M. Rasmussen, S. L. Anzick, M. R. Waters, P. Skoglund, M. DeGiorgio, T. W. Stafford Jr., S. Rasmussen, I. Moltke, A. Albrechtsen, S. M. Doyle, G. D. Poznik, V. Gudmundsdottir, R. Yadav, A. S. Malaspinas, S. S. White 5th, M. E. Allentoft, O. E. Cornejo, K. Tambets, A. Eriksson, P. D. Heintzman, M. Karmin, T. S. Korneliussen, D. J. Meltzer, T. L. Pierre, J. Stenderup, L. Saag, V. M. Warmuth, M. C. Lopes, R. S. Malhi, S. Brunak, T. Sicheritz-Ponten, I. Barnes, M. Collins, L. Orlando, F. Balloux, A. Manica, R. Gupta, M. Metspalu, C. D. Bustamante, M. Jakobsson, R. Nielsen, E. Willerslev, The genome of a Late Pleistocene human from a Clovis burial site in western Montana. *Nature* **506**, 225–229 (2014). doi:10.1038/nature13025 Medline

3. D. L. Jenkins, L. G. Davis, T. W. Stafford Jr., P. F. Campos, B. Hockett, G. T. Jones, L. S. Cummings, C. Yost, T. J. Connolly, R. M. Yohe 2nd, S. C. Gibbons, M. Raghavan, M. Rasmussen, J. L. Paijmans, M. Hofreiter, B. M. Kemp, J. L. Barta, C. Monroe, M. T. Gilbert, E. Willerslev, Clovis age Western Stemmed projectile points and human coprolites at the Paisley Caves. *Science* **337**, 223–228 (2012). doi:10.1126/science.1218443 Medline

4. F. A. Kaestle, D. G. Smith, Ancient mitochondrial DNA evidence for prehistoric population movement: The Numic expansion. *Am. J. Phys. Anthropol.* **115**, 1–12 (2001). doi:10.1002/ajpa.1051 Medline

5. B. M. Kemp, R. S. Malhi, J. McDonough, D. A. Bolnick, J. A. Eshleman, O. Rickards, C. Martinez-Labarga, J. R. Johnson, J. G. Lorenz, E. J. Dixon, T. E. Fifield, T. H. Heaton, R. Worl, D. G. Smith, Genetic analysis of early holocene skeletal remains from Alaska and its implications for the settlement of the Americas. *Am. J. Phys. Anthropol.* **132**, 605–621 (2007). doi:10.1002/ajpa.20543 Medline

6. J. A. Raff, D. A. Bolnick, Palaeogenomics: Genetic roots of the first Americans. *Nature* **506**, 162–163 (2014). doi:10.1038/506162a Medline

7. D. G. Steele, J. F. Powell, in *Who Were the First Americans?*, R. Bonnichsen, Ed. (Center for the Study of the First Americans, Oregon State University, Corvallis, OR, 1999), pp. 25–40.

8. R. González-José, W. Neves, M. M. Lahr, S. González, H. Pucciarelli, M. Hernández Martínez, G. Correal, Late Pleistocene/Holocene craniofacial morphology in Mesoamerican Paleoindians: Implications for the peopling of the New World. *Am. J. Phys. Anthropol.* **128**, 772–780 (2005). doi:10.1002/ajpa.20165 Medline

9. J. F. Powell, W. A. Neves, Craniofacial morphology of the first Americans: Pattern and process in the peopling of the New World. *Am. J. Phys. Anthropol.* **110** (suppl. 29), 153–188 (1999). doi:10.1002/(SICI)1096-8644(1999)110:29+<153::AID-AJPA6>3.0.CO;2-L Medline

10. C. G. Turner 2nd, Major features of Sundadonty and Sinodonty, including suggestions about East Asian microevolution, population history, and late Pleistocene relationships with Australian aboriginals. *Am. J. Phys. Anthropol.* **82**, 295–317 (1990). doi:10.1002/ajpa.1330820308 Medline

11. M. M. Lahr, History in the bones. *Evol. Anthropol.* **6**, 2–6 (1997).

12. J. C. Chatters, in *Human Variation in the Americas: The Integration of Archaeology and Biological Anthropology*, B. M. Auerbach, Ed. (Occasional Paper 38, Center for Archaeological Investigations, Southern Illinois Univ., Carbondale, IL, 2010), pp. 51–76.

13. J. F. Powell, *The First Americans: Race, Evolution, and the Origin of Native Americans* (Cambridge Univ. Press, Cambridge, 2004).

14. W. A. Neves, A. Hubbe, D. Bernardo, A. Strauss, A. Araujo, R. Kipnis, in *Paleoamerican Odyssey*, K. E. Graff, C. V. Ketron, M. R. Waters, Eds. (Center for the Study of the First Americans, College Station, TX, 2013), pp. 397–412.

15. W. R. Peltier, R. G. Fairbanks, Global glacial ice volume and Last Glacial Maximum duration from an extended Barbados sea level record. *Quat. Sci. Rev.* **25**, 3322–3337 (2006). doi:10.1016/j.quascirev.2006.04.010

16. B. J. Szabo, W. C. Ward, A. E. Weidie, M. J. Brady, Age and magnitude of Late Pleistocene sea-level rise on eastern Yucatan Peninsula. *Geology* **6**, 713–715 (1978).

17. G. A. Milne, M. Peros, Data-model comparison of Holocene sea-level change in the circum-Caribbean region. *Global Planet. Change* **107**, 119–131 (2013). doi:10.1016/j.gloplacha.2013.04.014

18. R. W. Graham, in *The World of Elephants (La Terra degli Elefanti)—Proceedings of the 1st International Congress (Atti del 1° Congreso Internazionale)*, G. Cavarretta *et al.*, Eds. (Consiglio Nazionale delle Ricerche, Rome, 2001), pp. 707–709.

19. G. Haynes, Extinctions in North America's late glacial landscapes. *Quat. Int.* **285**, 89–98 (2013). doi:10.1016/j.quaint.2010.07.026

20. E. Bard, B. Hamelin, D. Delanghe-Sabatier, Deglacial meltwater pulse 1B and Younger Dryas sea levels revisited with boreholes at Tahiti. *Science* **327**, 1235–1237 (2010). doi:10.1126/science.1180557 Medline

21. M. Medina-Elizalde, A global compilation of coral sea-level benchmarks: Implications and new challenges. *Earth Planet. Sci. Lett.* **362**, 310–318 (2013). doi:10.1016/j.epsl.2012.12.001

22. M. M. Lahr, *Evolution of Modern Human Diversity* (Cambridge Univ. Press, Cambridge, 1996).

23. U. A. Perego, N. Angerhofer, M. Pala, A. Olivieri, H. Lancioni, B. Hooshiar Kashani, V. Carossa, J. E. Ekins, A. Gómez-Carballa, G. Huber, B. Zimmermann, D. Corach, N. Babudri, F. Panara, N. M. Myres, W. Parson, O. Semino, A. Salas, S. R. Woodward, A. Achilli, A. Torroni, The initial peopling of the Americas: A growing number of founding mitochondrial genomes from Beringia. *Genome Res.* **20**, 1174–1179 (2010). doi:10.1101/gr.109231.110 Medline

24. M. de Saint Pierre, C. M. Bravi, J. M. Motti, N. Fuku, M. Tanaka, E. Llop, S. L. Bonatto, M. Moraga, An alternative model for the early peopling of southern South America revealed by analyses of three mitochondrial DNA haplogroups. *PLOS ONE* **7**, e43486 (2012). doi:10.1371/journal.pone.0043486 Medline

25. P. J. Reimer *et al*., IntCal13 and Marine09 radiocarbon age calibration curves, 0–50,000 years cal BP. *Radiocarbon* **55**, 1869–1887 (2013).

26. F. Attolini, 2007 - First year of Aktun Hu exploration. *AMCS Act. Newsl.* **33**, 95–98 (2010).

27. A. Nava-Blank, Hoyo Negro. *AMCS Act. Newsl.* **34**, 53–58 (2010).

28. W. D. Haglund, M. H. Sorg, in *Advances in Forensic Taphonomy. Method, Theory, and Archaeological Perspectives*, W. D. Haglund, M. H. Sorg, Eds. (CRC Press, Boca Raton, FL, 2002), pp. 201–275.

29. L. E. Sánchez Rojas, L. D. Barajas Nigoche, A. de la Calleja Moctezuma, *Carta Geológico-Minera, Estados de: Campeche, Quintana Roo, y Yucatán*, scale 1:500,000 (Servicio Geológico Mexicano, 2007).

30. P. Bauer-Gottwein, B. R. N. Gondwe, G. Charvet, L. E. Marín, M. Rebolledo-Vieyra, G. Merediz-Alonso, Review: The Yucatan Peninsula karst aquifer, Mexico. *Hydrogeol. J.* **19**, 507–524 (2011). doi:10.1007/s10040-010-0699-5

31. P. L. Smart, P. A. Beddows, J. Coke, J. S. Doerr, S. Smith, F. Whitaker, Cave development on the Caribbean coast of the Yucatan Peninsula, Quintana Roo, Mexico. *Geol. Soc. Am. Spec. Pap*. **404**, 105–128 (2006).

32. F. F. Whitaker, P. L. Smart, Characterizing scale-dependence of hydraulic conductivity in carbonates: Evidence from the Bahamas. *J. Geochem. Explor.* **69-70**, 133–137 (2000). doi:10.1016/S0375-6742(00)00016-9

33. E. Perry, J. Swift, J. Gamboa, A. Reeve, R. Sanborn, L. Marin, M. Villasuso, Geologic and environmental aspects of surface cementation, north coast, Yucatan, Mexico. *Geology* **17**, 818–821 (1989). doi:10.1130/0091-7613(1989)017<0818:GAEAOS>2.3.CO;2

34. QRSS, Quintana Roo Speleological Survey, List of Long Underwater Caves in Quintana Roo Mexico, www.caves.org/project/qrss/qrlong.htm, accessed 3 November 2013.

35. M. B. Bush, A. Y. Correa-metrio, D. A. Hodell, M. Brenner, F. S. Anselmetti, D. Ariztegui, A. D. Mueller, J. H. Curtis, D. A. Grzesik, C. Burton, A. Gilli, in *Past Climate Variability in South America and Surrounding Regions, from the Last Glacial*

Maximum to the Holocene, F. Vimeux, F. Sylvestre, M. Khodri, Eds., vol. 14 of *Developments in Paleoenvironmental Research* (Springer, Netherlands, 2009), pp. 113–128.

36. J. Escobar, D. A. Hodell, M. Brenner, J. H. Curtis, A. Gilli, A. D. Mueller, F. S. Anselmetti, D. Ariztegui, D. A. Grzesik, L. Pérez, A. Schwalb, T. P. Guilderson, A ~43-ka record of paleoenvironmental change in the Central American lowlands inferred from stable isotopes of lacustrine ostracods. *Quat. Sci. Rev.* **37**, 92–104 (2012). doi:10.1016/j.quascirev.2012.01.020

37. B. Leyden, M. Brenner, D. A. Hodell, H. Curtis, Late Pleistocene climate in the Central American lowlands. *Geophys. Monogr.* **78**, 165–178 (1993).

38. D. A. Hodell, F. S. Anselmetti, D. Ariztegui, M. Brenner, J. H. Curtis, A. Gilli, D. A. Grzesik, T. J. Guilderson, A. D. Müller, M. B. Bush, An 85-ka record of climate change in lowland Central America. *Quat. Sci. Rev.* **27**, 1152–1165 (2008). doi:10.1016/j.quascirev.2008.02.008

39. A. Correa-Metrio, M. B. Bush, K. R. Cabrera, S. Sully, M. Brenner, D. A. Hodell, J. Escobar, T. Guilderson, Rapid climate change and no-analog vegetation in lowland Central America during the last 86,000 years. *Quat. Sci. Rev.* **38**, 63–75 (2012). doi:10.1016/j.quascirev.2012.01.025

40. T. D. Dillehay, *The Settlement of the Americas* (Basic Books, New York, 2000).

41. A. J. Ranere, in *Paleoindian Archaeology: A Hemispheric Perspective*, J. Morrow, C. Gnecco, Eds. (Univ. of Florida Press, Gainesville, FL, 2006), pp. 69–85.

42. J. Arroyo-Cabrales, T. Alvarez, in *Ice Age Cave Faunas of North America*, B. W. Schubert, J. I. Mead, R. W. Graham, Eds. (Indiana Univ. Press and Denver Museum of Nature & Science, Denver, CO, 2003), pp. 262–272.

43. A. H. González, A. Terrazas, W. Stinnesbeck, M. E. Benavente, J. Avilés, C. Rojas, J. M. Padilla, A Velásquez, E. Acevez, E. Frey, in *Paleoamerican Odyssey*, K. E. Graf, C. V. Ketron, M. R. Waters, Eds. (Center for the Study of the First Americans, College Station, TX, 2013), pp. 223–238.

44. A. C. González González, C. Rojas Sandoval, A. Terrazas Mata, M. Benivente Sanvicente, W. Stinnesbeck, in *2° Simposio Internacional El Hombre Temprano en América* (IHAH, Ciudad de Mexico, Mexico, 2006), pp. 73–90.

45. R. E. Taylor, Six decades of radiocarbon dating in New World archaeology. *Radiocarbon* **51**, 173–212 (2009).

46. Prep-Laboratory Staff, Internal technical reports, Keck Carbon Cycle Accelerator Mass Spectrometer Laboratory, University of California, Irvine (2010); www.ess.uci.edu/researchgrp/ams/protocols.

47. G. M. Santos, S. R. Southon, K. C. Druffel-Rodriguez, S. Griffin, M. Mazon, Magnesium perchlorate as an alternative water trap in AMS graphite sample preparation: A report on sample preparation at the KCCAMS facility at the University of California, Irvine. *Radiocarbon* **46**, 165–173 (2004).

48. G. M. Santos, J. R. Southon, S. Griffin, S. R. Beaupre, E. R. M. Druffel, Ultra small mass AMS ^{14}C sample preparation and analyses at KCCAMS/UCI Facility. *Nucl. Instrum. Methods Phys. Res.* **259**, 293–302 (2007). doi:10.1016/j.nimb.2007.01.172

49. M. Stuiver, H. A. Polach, Discussion: Reporting of ^{14}C data. *Radiocarbon* **19**, 355–363 (1977).

50. C. Bronk Ramsey, Bayesian analysis of radiocarbon dates. *Radiocarbon* **51**, 337–360 (2009).

51. U. Zoppi, J. Crye, Q. Song, A. Arjomand, Performance evaluation of the new AMS system at Accium Biosciences. *Radiocarbon* **49**, 173–182 (2007).

52. G. K. Ward, S. R. Wilson, Procedures for comparing and combining radiocarbon age determinations: A critique. *Archaeometry* **20**, 19–31 (1978). doi:10.1111/j.1475-4754.1978.tb00208.x

53. R. E. Taylor, *Radiocarbon Dating: An Archaeological Perspective* (Academic Press, New York, 1987).

54. A. Zazzo, J. F. Saliège, Radiocarbon dating of biological apatites: A review. *Palaeogeogr. Palaeoclimatol. Palaeoecol.* **310**, 52–61 (2011). doi:10.1016/j.palaeo.2010.12.004

55. R. E. M. Hedges, J. A. Lee-Thorp, N. C. Tuross, Is tooth enamel carbonate a suitable material for radiocarbon dating? *Radiocarbon* **37**, 285–290 (1995).

56. D. R. Piperno, in *Tropical Rainforest Responses to Climate Change*, M. B. Bush, J. Flenley, Eds. (Praxis Publishing, Chichester, UK, 2007), pp. 193–218.

57. T. W. Stafford Jr., P. E. Hare, L. Currie, A. J. T. Jull, D. J. Donahue, Accelerator radiocarbon dating at the molecular level. *J. Archaeol. Sci.* **18**, 35–72 (1991). doi:10.1016/0305-4403(91)90078-4

58. T. W. Stafford Jr., K. Brendel, R. Duhamel, Radiocarbon, ^{13}C and ^{15}N analysis of fossil bone: Removal of humates with XAD-2 resin. *Geochim. Cosmochim. Acta* **52**, 2257–2267 (1988). doi:10.1016/0016-7037(88)90128-7

59. C. Hill, P. Forti, *Cave Minerals of the World* (National Speleological Society, Huntsville, AL, ed. 2, 1997).

60. K. R. Ludwig, *User's Manual for Isoplot/Ex, Version 2.49: A Geochronological Toolkit for Microsoft Excel* (Berkeley Geochronology Center Special Publication No. 1a, Berkeley Geochronology Center, Berkeley, CA, 2001).

61. Y. Asmerom, V. J. Polyak, S. J. Burns, Variable winter moisture in the southwestern United States linked to rapid glacial climate shifts. *Nat. Geosci.* **3**, 114–117 (2010). doi:10.1038/ngeo754

62. H. Cheng, R. L. Edwards, C.-C. Shen, V. J. Polyak, Y. Asmerom, J. Woodhead, J. Hellstrom, Y. Wang, X. Kong, C. Spötl, X. Wang, E. Calvin Alexander Jr., Improvements in 230 Th dating, ^{230}Th and ^{234}U half-life values, and U-Th isotopic measurements by multi-collector inductively coupled plasma mass spectrometry. *Earth Planet. Sci. Lett.* **371-372**, 82–91 (2013). doi:10.1016/j.epsl.2013.04.006

63. J. S. Oslick, K. G. Miller, M. D. Feigenson, J. D. Wright, Oligocene-Miocene strontium isotopes: Stratigraphic revisions and correlations to an inferred glacioeustatic record. *Paleoceanography* **9**, 427–443 (1994). doi:10.1029/94PA00249

64. W. M. Bass, *Human Osteology: A Laboratory and Field Manual* (Missouri Archaeological Society, Columbia, MO, ed. 3, 1987).

65. J. E. Buikstra, D. H. Ubelaker, *Standards for Data Collection from Human Skeletal Remains* (Arkansas Archaeological Survey, Fayetteville, AR, 1994).

66. D. H. Ubelaker, *Human Skeletal Remains, Excavation, Analysis, Interpretation* (Aldine, Chicago, IL, 1978).

67. C. F. Moorrees, E. A. Fanning, E. E. Hunt, Jr., Age variation of formation stages for ten permanent teeth. *J. Dent. Res.* **42**, 1490–1502 (1963). doi:10.1177/00220345630420062701 Medline

68. M. Schaefer, S. Black, L. Scheuer, *Juvenile Osteology* (Academic Press, Boston, MA, 2009).

69. B. J. Baker, T. L. Dupras, M. W. Tochert, *The Osteology of Infants and Children* (Texas A&M Press, College Station, TX, 2005).

70. S. Genovés, Proportionality of the long bones and their relation to stature among Mesoamericans. *Am. J. Phys. Anthropol.* **26**, 67–77 (1967). doi:10.1002/ajpa.1330260109 Medline

71. M. Bastir, A. Rosas, P. O'Higgins, Craniofacial levels and the morphological maturation of the human skull. *J. Anat.* **209**, 637–654 (2006). doi:10.1111/j.1469-7580.2006.00644.x Medline

72. D. G. Steele, in *Wilson Leonard: An 11,000 Year Record of Hunter-Gatherers in Central Texas*, M. Collins, Ed. (Texas Archaeological Research Laboratory, Austin, TX, 1998), pp. 1141–1158.

73. S. Hillson, *Dental Anthropology* (Cambridge Univ. Press, Cambridge, 1959).

74. C. G. Turner II, C. R. Nichol, G. R. Scott, in *Advances in Dental Anthropology*, M. A. Kelly, C. S. Larsen, Eds. (Willey-Liss, New York, 1991), pp. 11–31.

75. J. F. Powell, Dental evidence for the peopling of the New World: Some methodological considerations. *Hum. Biol.* **65**, 799–819 (1993). Medline

76. B. M. Kemp, C. Monroe, D. G. Smith, Repeat silica extraction: A simple technique for the removal of PCR inhibitors from DNA extracts. *J. Archaeol. Sci.* **33**, 1680–1689 (2006). doi:10.1016/j.jas.2006.02.015

77. C. Grier, K. Flanigan, M. Winters, L. G. Jordan, S. Lukowski, B. M. Kemp, Using ancient DNA identification and osteometric measures of archaeological Pacific salmon vertebrae for reconstructing salmon fisheries and site seasonality at Dionisio Point, British Columbia. *J. Archaeol. Sci.* **40**, 544–555 (2013). doi:10.1016/j.jas.2012.07.013

78. C. Monroe, C. Grier, B. M. Kemp, Evaluating the efficacy of various thermo-stable polymerases against co-extracted PCR inhibitors in ancient DNA samples. *Forensic Sci. Int.* **228**, 142–153 (2013). doi:10.1016/j.forsciint.2013.02.029 Medline

79. A. Ginolhac, M. Rasmussen, M. T. Gilbert, E. Willerslev, L. Orlando, mapDamage: Testing for damage patterns in ancient DNA sequences. *Bioinformatics* **27**, 2153–2155 (2011). doi:10.1093/bioinformatics/btr347 Medline

80. S. Lindgreen, AdapterRemoval: Easy cleaning of next-generation sequencing reads. *BMC Res. Notes* **5**, 337–345 (2012). doi:10.1186/1756-0500-5-337 Medline

81. R. M. Andrews, I. Kubacka, P. F. Chinnery, R. N. Lightowlers, D. M. Turnbull, N. Howell, Reanalysis and revision of the Cambridge reference sequence for human mitochondrial DNA. *Nat. Genet.* **23**, 147 (1999). doi:10.1038/13779 Medline

82. H. Li, R. Durbin, Fast and accurate short read alignment with Burrows-Wheeler transform. *Bioinformatics* **25**, 1754–1760 (2009). doi:10.1093/bioinformatics/btp324 Medline

83. H. Li, B. Handsaker, A. Wysoker, T. Fennell, J. Ruan, N. Homer, G. Marth, G. Abecasis, R. Durbin; 1000 Genome Project Data Processing Subgroup, The sequence alignment/map format and SAMtools. *Bioinformatics* **25**, 2078–2079 (2009). doi:10.1093/bioinformatics/btp352 Medline

84. Z. Wei, W. Wang, P. Hu, G. J. Lyon, H. Hakonarson, *SNVer*: A statistical tool for variant calling in analysis of pooled or individual next-generation sequencing data. *Nucleic Acids Res.* **39**, e132 (2011). doi:10.1093/nar/gkr599 Medline

85. D. A. Bolnick, H. M. Bonine, J. Mata-Míguez, B. M. Kemp, M. H. Snow, S. A. LeBlanc, Nondestructive sampling of human skeletal remains yields ancient nuclear and mitochondrial DNA. *Am. J. Phys. Anthropol.* **147**, 293–300 (2012). doi:10.1002/ajpa.21647 Medline

86. V. J. Polyak, Y. Asmerom, S. J. Burns, M. S. Lachniet, Climatic backdrop to the terminal Pleistocene extinction of North American mammals. *Geology* **40**, 1023–1026 (2012). doi:10.1130/G33226.1

87. J. Chapman, *The Icehouse Bottom Site 40MR73* (Report of Investigations 13**,** Department of Anthropology, University of Tennessee, Knoxville, TN, 1973).

88. A. L. Kroeber, The Rancho La Brea skull. *Am. Antiq.* **27**, 416–419 (1962). doi:10.2307/277805

89. R. Berger, Advances and results in radiocarbon dating: Early man in America. *World Archaeol.* **7**, 174–184 (1975). doi:10.1080/00438243.1975.9979631 Medline

90. S. C. Kuzminsky, thesis, University of California, Santa Barbara,CA, 2013).

91. A. Dansie, Early Holocene burials in Nevada: Overview of localities, research, and legal issues. *Nev. Hist. Soc. Q.* **40**, 1–14 (1997).

92. D. Tuohy, A. Dansie, New information regarding early Holocene manifestations in the western Great Basin. *Nev. Hist. Soc. Q.* **40**, 24–53 (1997).

93. E. J. Dixon, *Bones, Boats and Bison* (Univ. of New Mexico Press, Albuquerque, NM, 1999).

94. H. J. H. Edgar, Paleopathology of the Wizard's Beach Man and Spirit Cave Mummy. *Nev. Hist. Soc. Q.* **40**, 57–61 (1997).

95. W. A. Neves, M. Hubbe, G. Correal, Human skeletal remains from Sabana de Bogotá, Colombia: A case of Paleoamerican morphology late survival in South America? *Am. J. Phys. Anthropol.* **133**, 1080–1098 (2007). doi:10.1002/ajpa.20637 Medline

96. R. L. Jantz, D. W. Owsley, Pathology, taphonomy, and cranial morphometrics of the Spirit Cave Mummy. *Nev. Hist. Soc. Q.* **40**, 62–84 (1997).

97. G. S. Krantz, Oldest human remains from the Marmes Site. *Northwest Anthropological Res. Notes* **13**, 159–173 (1979).

98. B. Hicks, Ed., *Marmes Rockshelter: A Final Report on 11,000 Years of Cultural Use* (Washington State Univ. Press, Pullman, WA, 2004).

99. D. Young, S. Patrick, D. G. Steele, An analysis of the Paleoindian double burial from Horn Shelter No. 2, in Central Texas. *Plains Anthropol.* **32**, 275–298 (1987).

100. C. B. Bousman, in *Wilson Leonard: An 11,000 Year Record of Hunter Gatherers in Central Texas*, M. Collins, Ed. (Studies in Archaeology 31**,**Texas Archaeological Research Laboratory, Austin, TX, 1998), pp. 161–210.

101. D. A. Breternitz, A. C. Swedlund, D. C. Anderson, An early burial from Gordon Creek, Colorado. *Am. Antiq.* **36**, 170–182 (1971). doi:10.2307/278669

102. D. W. Owsley, M. A. Jodry, T. W. Stafford, C. V. Haynes Jr., D. J. Stanford, *Arch Lake Woman* (Texas A&M Press, College Station, TX, 2010).

103. S. Gonzalez, J. C. Jiménez-López, R. Hedges, D. Huddart, J. C. Ohman, A. Turner, J. A. Pompa y Padilla, Earliest humans in the Americas: New evidence from México. *J. Hum. Evol.* **44**, 379–387 (2003). doi:10.1016/S0047-2484(03)00004-6 Medline

104. T. J. Green, B. Cochran, T. W. Fenton, J. C. Woods, G. L. Titmus, L. Tieszen, M. A. Davis, S. J. Miller, The Buhl Burial: A Paleoindian woman from southern Idaho. *Am. Antiq.* **63**, 437–456 (1998). doi:10.2307/2694629

105. J. C. Jiménez López, H. Hernández Flores, G. Martínez Sosa, G. Saucedo Arteaga, in *El Hombre Temprano en América y sus Implicaciones en el Poblamiento de la Cuenca de México* (INAH, Ciudad de México, Mexico, 2006), pp. 49–66.

106. J. R. Johnson, T. W. Stafford Jr., H. O. Ajie, D. P. Morris, in *Proceedings of the Fifth California Islands Symposium*, D. R. Brown, K. C. Mitchell, H. W. Chaney, Eds. (OCS Study MMS 99-0038, U.S. Department of the Interior Minerals Management Service, Pacific Outer Continental Shelf Region, 2002), pp. 541–545.

107. J. Feathers, R. Kipnis, M. Aroyo-Kalin, D. Koblenz, How old is Luzia: Luminescence dating and stratigraphic integrity at Lapa Vermelha, Lagoa Santa, Brazil. *Geoarchaeol.* **25**, 395–436 (2010).